2022 Quick Review of Fine Needle Aspiration Accuracy with Focus on Cytohistologic Correlation and Evaluation of Discrepant Cases in a Limited Sample

Somaye Yekezare, Niloufar Reisian, Xiaoyan Liao, Farnaz Hasteh. University of California San Diego Health System, San Diego, CA; Kaiser Medical Center, San Diego, CA.

Background: Fine needle aspiration biopsy (FNAB) is a minimally invasive procedure commonly utilized for the primary investigation of mass lesions. Correlation of FNAB diagnosis with histopathologic results is part of quality assurance and quality control in cytology laboratories. The aim of this study was to investigate the diagnostic performance of FNAB and to identify the specimen types that are prone to errors.

Design: A total of 1125 FNABs performed at our institutes in 2013 were selected and 401 satisfactory cases with the follow-up surgical specimens were included for this study. FNAB results were classified as negative, atypia, or positive; whereas final pathologic diagnoses were classified as malignant or benign. The cases were categorized into lymph nodes (n=124), lung and chest (n=71), GI tract and liver (n=58), pancreatobiliary tract (n=45), thyroid (n=42), head and neck (n=34), bone and soft tissue (n=17), and genitourinary (n=10). Fifteen (3.7%) cases with discordant diagnosis on follow up samples were identified. The discrepant cases were reviewed by two cytopathologists blindly and their diagnoses were compared to the original results. Discrepancies of these cases were classified as interpretive or possibly sampling errors.

Results: Cytology diagnosis was confirmed by histology in 386 of 401 FNABs (96.3%). Only 15 cases were discrepant and review of these cases showed 9 cases were misdiagnosed originally (interpretation errors 60%). The remaining 6 cases were diagnosed correctly and did not represent the lesion, most likely due to sampling error (40%). Thyroid (9.5%) followed by pancreaticobiliary tract (6.6%) had the highest interpretive discrepancy rates; whereas head and neck accounted for the highest sampling errors (5.8%). Fisher's exact test yielded no significant differences in discrepancy rates for different specimen types (P>0.05). Among the 15 discrepant cases, 11 were undercalled as benign or atypia (80%) and three were overcalled as positive (20%). Only 3 cases with interpretive errors were reviewed by other pathologists as a second opinion (33%).

Conclusions: FNAB has an excellent correlation with surgical pathology results and is an effective procedure for the diagnosis of mass lesions. The accuracy of this highly reliable tool can be further improved with accurate sampling. Interpretive errors can be minimized by careful examination of the cytologic findings and intradepartmental consultation.

2023 Improving Utilization of Hemochromatosis Testing

Yaolin Zhou, Gary Procop, Jacquelyn Riley. Cleveland Clinic, Cleveland, OH.

Background: HFE hemochromatosis (HFE-HC) due to homozygous C282Y mutations in the *HFE* gene is a well-known cause of inherited iron overload syndrome, yet disease penetrance is low and iron studies are non-specific. We integrated international practice guidelines with our clinical data for the evaluation of patients with suspected HFE-HC.

Design: To assess routine practice at our institution, we performed a retrospective review of 566 *HFE* orders and a subset analysis of 55 consecutive orders and all HFE-HC patients. These were compared with European guidelines, which encourage step-wise evaluation of hyperferritinemia, and U.S. guidelines, which recommend genetic testing of patients with abnormal iron studies or a positive family history.

Results: Results from 1/6/2015 to 8/3/2015 showed 4.6% C282Y/C282Y, 12% C282Y carriers, 5% C282Y/H63D, and 77% non-risk genotypes. Only C282Y/C282Y patients have significant risk for iron overload. Five HFE-HC patients had a positive family history. At least 7 tests were ordered on known HFE-HC patients (new diagnosis rate <3.5%).

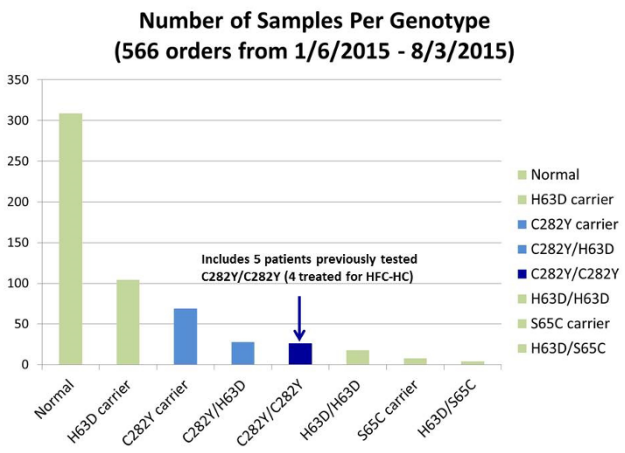

Of 43 *HFE* orders from 7/20-8/3/2015, gastroenterologists and generalists ordered tests most frequently. Seventeen patients had liver disease, e.g. cirrhosis (6), viral hepatitis (5), fatty liver (4), acute alcohol intoxication (2) and transfusion-related iron overload (2). Patients with non-risk genotypes had lower mean serum ferritin (613 ng/mL vs. 1,070 ng/mL, $p=0.03$) and transferrin saturation (43% vs. 66%, $p<0.01$) than those with C282Y genotypes. The recommended criterion of TS>45% was 94% sensitive in identifying patients with C282Y and 100% sensitive for C282Y/C282Y. Serum ferritin>1,000 mcg/L, which correlates with cirrhosis, was 76% specific for C282Y. Most C282Y heterozygotes (4) and C282Y/C282Y (13) patients with available results met these cut offs, and two C282Y patients met criteria based on family history alone.

Conclusions: The proposed criteria of TS>45%, ferritin>1,000 mcg/L, or a positive family history, was 100% sensitive and moderately specific for C282Y screening. Our institution is now considering an approach to include measuring ferritin/TS, and reflexive *HFE* gene testing only when criteria are met. If used broadly, the algorithm should detect all at-risk patients and result in an estimated 43% reduction of unnecessary *HFE* tests and a lower cost per new diagnosis.

Techniques (including Ultrastructure)

2024 Complementary Value of Electron Microscopy and Immunohistochemistry in the Diagnosis of Non-Small Cell Lung Cancer

Raquel Albero, Lara Pijuan, Mercedes Simon, Nuria Juanpere, Ivonne Vazquez, Adria Lloret, Jessica Munne, Ignacio Sanchez, Sergio Serrano, Josep Lloreta. Hospital del Mar, Barcelona, Spain; Istituto Clinico Humanitas, Milan, Italy; Autonomous University of Barcelona, Barcelona, Spain; Pompeu Fabra University, Barcelona, Spain.

Background: Pathological classification of lung cancer has been redefined by cytogenetics and molecular data. Consequently, therapeutic targets have been identified for pulmonary adenocarcinoma (ADK). Thus, it is crucial to accurately distinguish between ADK and squamous cell carcinoma (SQCC) in poorly differentiated cases. Immunohistochemistry (IHC) is very helpful in making this differential diagnosis. However, a subset of cases remains classified as Non-Small Cell Lung Carcinoma, NOS (NSCLC-NOS), after IHC. In these cases, Electron Microscopy (EM) can be a useful tool, as it objectively identifies glandular differentiation. The aim of this study was to determine the value of EM and IHC in the NSCLC-NOS subclassification.

Design: Forty-eight NSCLC-NOS cases were selected from the files of Parc de Salut Mar Biobank, Barcelona, Spain. IHC panel consisted of TTF-1 and p40 antibodies, and for older cases, p63 was available. Tissue was retrieved from paraffin blocks and processed for EM. The results of each technique were compared to the final diagnosis (gold standard), that was derived from the combination of light microscopy, IHC, EM, cytogenetics, molecular studies and data of the resection specimen if available.

Results: IHC concurred with the final diagnosis in 38 cases (79.2%) (Kappa=0.517). The identification of ADK by IHC had a sensitivity of 73%, specificity of 100%, positive predictive value (PPV) of 100% and negative predictive value (NPV) of 52.4%. EM results agreed with the final diagnosis in 35 cases (72.9%) (Kappa=0.471). For the diagnosis of ADK, IHC failed to recognize 10 cases (TTF1, P40 negative) and in all of them EM was conclusive, while in 10 cases with inconclusive EM, IHC gave the diagnosis. Thus, the values obtained for EM were identical to those of IHC: sensitivity 73%, specificity 100%, PPV 100% and NPV 52.4%. Combining results of IHC and EM, 47 cases (97.9%) were coincident with the final diagnosis (Kappa=0.943).

Conclusions: The results of this retrospective study support that EM can provide useful information in the diagnosis of NSCLC, mainly in recognizing poorly differentiated ADK, and that it has a particularly helpful role in cases in which IHC provides inconclusive results.

2025 Colour Deconvolution Is Superior to Hue-Saturation-Intensity in Digital Analysis of Atherosclerotic Plaques

Murad Alturkustani, J David Spence, Catherine Currie, Myra Cocker, Cathie Crukley, Martin J Yaffe, Jean-Claude Tardif, Cheemun Lum, Robert Beanlands, Robert Hammond, Ali Khan. King Abdulaziz University, Jeddah, Saudi Arabia; London Health Sciences Centre and Lawson Research Institute, London, Canada; University of Western Ontario, London, Canada; Robarts Research Institute, London, Canada; Ottawa Heart Institute, Ottawa, Canada; Montreal Heart Institute, Montreal, Canada; Sunnybrook Health Sciences Centre, Toronto, Canada.

Background: Digital analysis is becoming an essential tool in the quantitative analysis of immunohistochemically stained slides. The positive pixel algorithm is a widely applied method, built into the Aperio ImageScope software, and uses the Hue-Saturation-Intensity (HSI) colour-space to segment positively-stained pixels. An alternative approach, using colour deconvolution (CD), decomposes the image into separate channels for each stain using predefined colour samples. We sought to compare these two approaches

Design: This is a sub-study under the Canadian Atherosclerosis Imaging Network (CAIN) project of carotid plaque analysis that aims to improve the assessment of carotid atheromatous disease through studies that inform clinical imaging with gold-standard data (plaque pathology). One study component is to electronically annotate CD68 immunostained slides in atherosclerotic plaques for comparison with ultrasound, CT and PET data. Carotid endarterectomy specimens were sub-serially sectioned, stained, digitized and annotated manually and by electronic algorithms for CD68 immunostain. A set of 60 CD68-stained fields (from randomized subjects and slides) with corresponding segmentations (HSI, and CD) were examined in a blinded fashion by two neuropathologists (MA, RH). The neuropathologists were asked to choose the segmentation that best represented the labeling of positively stained tissue on the slide.

Results: The two observers found CD superior 94-100% of the time. It was also observed that the HSI algorithm did not identify the most heavily stained regions on the slide. This could be due to an innately poor ability to resolve differences in hue (H) when the intensity (I) is very low.

Conclusions: Colour deconvolution algorithms appear superior to those based on hue-saturation-intensity, especially in heavily-stained regions of the image.

2026 RNAscope® 2.5: A Robust and High Performance RNA In Situ Hybridization Assay for Formalin-Fixed Paraffin-Embedded Tissue

Courtney Anderson, Li-chong Wang, Casey Kernag, Bingqing Zhang, Emerald Butko, Melanie Miller, Thomas Laver, Nan Su, Henry G Lamparski, Emily Park, Yuling Luo, Xiao-Jun Ma. Advanced Cell Diagnostics, Hayward, CA.

Background: RNA is a key biomarker of the dynamic gene expression changes occurring in cells and tissues. Compared to techniques that analyze bulk tissue, identifying RNA expression at the single cell level within the morphological context provides additional information, such as identifying the precise cellular and sub-cellular location of RNA, which can be highly valuable for the validation of high-throughput expression analyses. However, sensitivity and specificity are frequent concerns with traditional RNA *in situ* hybridization (ISH). RNAscope® is a novel ISH technology that overcomes these challenges, and RNAscope® 2.5 incorporates several improvements for enhanced robustness and performance.

Design: RNAscope® 2.5 assay was performed on forty-one deidentified archival formalin-fixed paraffin embedded (FFPE) human tissues, including breast, cervix, larynx, lung, lymph node, skin, and stomach, using three platforms: manual, Leica BOND RX, and Ventana Discovery ULTRA and XT. Signal-to-noise ratio was determined by examining staining for the negative control probe *dapB* and positive control probe Hs-*PPIB*. Reproducibility was assessed by examining the staining for *dapB* and Hs-*TBP* or Hs-*POLR2A*. RNAscope 2.5 signal quantification was performed using the Halo imaging analysis software (Indica Labs).

Results: Using the RNAscope® 2.5 assay on the Leica and Ventana automated platforms, we observed little to no background with *dapB* in a range of human tissues. Conversely, staining for *PPIB* showed intense, punctate spots in multiple human tissues, demonstrating a high signal-to-noise ratio. Across three reagent lots and three assay runs using manual and automated assays, no background was observed with *dapB*, while strong, consistent staining was observed with *TBP*. Examination of forty-one tissues encompassing seven tissue types with RNAscope® 2.5 on both manual and automated platforms demonstrated the utilization of one standard pretreatment condition for the tissues tested in this study. Equivalent staining across manual, Leica, and Ventana platforms was observed for *dapB* and *POLR2*A in cervix, lung, and skin tissues.

Conclusions: Here we present our latest technology, RNAscope® 2.5, demonstrating a high signal-to-noise ratio, product reproducibility and consistency, and a robust, quantifiable assay applicable for virtually any target in any tissue on manual and automated platforms. In particular, RNAscope® 2.5 should facilitate rapid assay development for translational research and shows a strong potential for further use in clinical research applications.

2027 Lesson Learned from the Evaluation of MYC Non-IGH Translocation Partners in DLBCL- An Institutional Experience

Renu Bajaj, Alexander Graham, Jerald Gong, Zi-Xuan Wang, Stephen C Peiper, Guldeep Uppal. Thomas Jefferson University Hospital, Philadelphia, PA.

Background: *MYC* rearrangement (*MYC*-R) occurs in 7-21% of DLBCL, involving either the immunoglobulin heavy chain (*IGH*) or Immunoglobulin light chain (*IGK* or *IGL*) and non-IG partners. Increased LDH level is one of the important prognostic markers based on International Prognostic Indices (IPIs). A few studies have reported *MYC*-R as an adverse molecular prognostic marker and a close association with increased serum lactate dehydrogenase (LDH) levels. We evaluated the status of *MYC* translocation partners in DLBCL patients and correlated with serum LDH level.

Design: Cases with a diagnosis of DLBCL were retrieved from the database of the department of Pathology presenting during last 3 years. A total of 9 cases with Fluorescence in situ hybridization (FISH) result with *MYC, BCL2* and *BCL6* gene rearrangements were selected for the study. 8 cases with *MYC*-R were tested for *IGK* and *IGL* rearrangement using break-apart probes. The cut off value was ≥ 7% positive cells. 1 case positive for *MYC-IGH* translocation was used as a control for comparing the LDH value.

Results: FISH results for *IGK* and *IGL* for 8 DLBCL patients with *MYC*-non *IG* rearrangements are shown in the following table:

Table 1

Case	FISH results (gene rearrangement)	IGL rearrangement	IGK rearrangement	Treatment	LDH (IU/L)	Status
1	BCL6 and MYC	-	-	4xRCHOP/Ara-C, BOCE, ICE, Rituximab	1130	Deceased
2	MYC	+	+	2xHyper-CVAD/IT then allogeneic SCT	209	Palliative care
3	MYC, BCL2/IGH	+	+	RCHOPx4	397	Remission
4	MYC, BCL6, BCL2	+	-	EPOCH	352	Deceased
5	MYC, BCL2/IGH	-	-	RCHOPx6, autologous HSCT	1279	On treatment
6	MYC, BCL2/IGH	+	-	RCHOPx6, Rituximab, MTXx4	213	Relapse
7	MYC, BCL6	-	+	2xR-CHOP/MTX	221	Remission
8	MYC, BCL2	-	-	1xRCHOP	2160	On treatment
9 (Control)	MYC/IGH	NA	NA	EPOCH	20460	Deceased

Conclusions: 5/8 cases (62.5%) with *MYC*-R and negative *MYC/IGH* showed *IGK* and/or *IGL* rearrangement. 3 positive cases (3/8) showed a LDH value within reference range while 2 showed only mild elevation (<400 IU/L), unlike DLBCL, NOS which frequently shows high LDH levels. This information could be the basis for an extended collaborative study to detect the prognostic implication of *MYC-IG* vs *MYC*-non *IG* partners. Reflex FISH testing to determine the status of *IGK* and *IGL* in MYC non-*IG* cases would be beneficial in DLBCL patients.

2028 Utility of Adenosine Diphosphate (ADP) Inhibition by Thromboelastography with Platelet Mapping (TEG-PM) in Predicting Hemorrhagic Stroke in a Level 1 Stroke Center: Analysis and Review of Literature

Kelly A Bowers, Richard D Hammer. University of Missouri, Columbia, MO.

Background: Early thrombolytic therapy in stroke is critical for improved outcomes and mortality. Indications for thrombolysis differ between hemorrhagic (HS) and ischemic (IS) strokes, which typically rely on CT or MRI. A rapid test that differentiates IS from HS to facilitate management in stroke patients is needed. Thromboelastography (TEG) with platelet mapping (TEG-PM) evaluates functional clot formation and lysis with real-time. We evaluated a cohort of patient at a level 1 stroke center regarding the use of TEG-PM and compared it to prior published criteria of TEG to evaluate IS and HS.

Design: 732 patients who had TEG performed at a level 1 stroke hospital were examined retrospectively. 206 patients met inclusion criteria, including coded diagnosis of IS or HS and confirmed diagnosis by CT/MRI. The final sample size was 118 patients, including 71 radiologic-confirmed IS and 47 radiologic-confirmed HS. Of those TEG-PM for ADP was available in 60 IS and 34 HS. Results of our cohort were also analyzed using previously published criteria of Handa (1999), Elliott (2015), Ettinger (1974), Zheng (2013), Kashuk (2009), and Kawano-Castillo (2014).

Results: ADP inhibition by TEG-PM was independently predictive of HS vs. IS. ($p=0.0347$; HS mean 54.76 ± 28.3 vs. IS mean 41.9 ± 28.4). A cutoff of 50% ADP inhibition was significant ($p=0.0494$). Fisher exact test and ROC analysis showed a sensitivity of 55.8%, specificity of 66.7%, PPV of 47.7% and NPV of 72.0%. Additionally, data supported findings found in four other studies. Ettinger (1974) and Elliott (2015) demonstrated IS were associated with increased MA and angle and decreased r and K on the basic TEG platform. There was a statistically significant difference ($p=0.0179$) between HI and IS using the Ettinger ratio (MA/r+K). Paradoxically, higher ratios were seen in HS, which were not studied in the original report (mean ratio HS 13.31 ± 9.12; vs IS 10.30 ± 4.33). Data also supported Zheng (2013). which showed modifications to TEG cut off indices could improve prediction and differentiation of IS and HS.

Conclusions: ADP inhibition by TEG-PM is a powerful tool in predicting the likelihood of HS vs. IS. Also this study validates the usefulness of the Ettinger ratio in strokes. Other TEG parameters demonstrate a significant reproducible difference in HI vs. IS. ADP inhibition, especially when correlated with other TEG values, offers rapid initial risk assessment of stroke patients and can predict HS.

2029 A Comparison of Manual Counting with Camera Captured Images and Digital Image Analysis for Ki-67 Proliferative Index Assessment in Pancreatic Neuroendocrine Tumors

Elliott Burdette, Charles Myers, Geoffrey Smith, Cameron Neely, Abigail L Goodman, Diane Lawson, Cynthia Cohen. Emory University School of Medicine, Atlanta, GA.

Background: Pathologic grading of pancreatic neuroendocrine tumors (PanNETs) currently is based on quantification of Ki-67 proliferative index (Ki-67 PI) for prognostic stratification under WHO 2010 guidelines. Methods of Ki-67 PI assessment include manual counting, “eyeball estimate”, manual count of camera captured images, and digital image analysis. The adaptation, efficiency, and accuracy of these methods vary by institution and pathologist. In this study, manual counting of camera captured images and digital image analysis methodologies were compared for Ki-67 PI in an evaluation of a series of PanNET cases to assess concordance.

Design: Fifty-seven PanNETs were analyzed using two methods: I) An expert pathologist examined a representative Ki-67 IHC stained slide. Six hotspots (areas of high Ki-67 positivity) were selected, a field containing each hotspot was photographed and printed for manual counting of Ki-67 positive and negative cells. II) Digital image analysis examined the same slide used for manual counting. A whole slide image was created using an Aperio ImageScope slide scanner. The resulting image was manually reviewed and six hotspots were selected and analyzed with the Aperio immunohistochemistry nuclear quantitative image analysis algorithm, which generated a Ki-67 PI and total nuclear count. The Ki-67 PI for each case was recorded and statistical analyses were performed to assess the concordance of the methods.

Results: Pathologic grade was concordant in 47/57 cases (82.4%). Of the 47 concordant cases, 27 (57.4%) cases’ Ki-67 PI was within 1 percent by both methods. Of 10 discordant cases, 2 changed from Grade 3 to Grade 2. A paired T test with two tails was performed ($p = 0.66$). Pearson’s correlation coefficient was performed ($r^2=0.7518$ and two tailed p value < 0.0001). The mean total nuclear count of the Aperio IHC algorithm was 6761 (range 1083-23263).

Conclusions: This study illustrates that digital image analysis is an acceptable method of Ki-67 PI assessment and grading of PanNETs when compared to manual count of camera captured images. The assessment of Ki-67 PI and resultant pathologic grade by manual counting of camera captured images was concordant with digital image analysis derived Ki-67 PI.

2030 Fusion Gene Detection in Sarcomas by the NanoString nCounter Fusion Gene Analysis Assay

Kenneth Chang, Angela Goytain, Xiu Qing Wang, Tony Ng. KK Women's and Children's Hospital, Singapore, Singapore; Duke-NUS Graduate Medical School, Singapore, Singapore; University of British Columbia, Vancouver, BC, Canada; Vancouver General Hospital, Vancouver, BC, Canada.

Background: About one-third of sarcomas express recurrent fusion oncogenes, identification of which is important for pathological diagnosis and patient management. Current methods for gene fusion detection include fluorescent in-situ hybridization (FISH) and reverse-transcriptase polyermase chain reaction (RTPCR), but these methods lack multiplex capabilities. The NanoString nCounter assay is a high-throughput hybridization technique using a custom-designed pooled code-set which can identify multiple gene fusions in a single assay. In this study, we assess the value of the NanoString assay in fusion gene identification in patient samples.

Design: We designed a customized pan-sarcoma code-set targeting 166 unique fusion junctions. The study cohort comprised resections and core biopsies of 34 soft tissue tumors of which 17 cases had known fusion genes (by FISH or RTPCR) and 17 cases had no pre-existing known fusion gene information. RNA extracted from formalin-fixed paraffin-embedded (FFPE) tissue was hybridized with the custom-designed code-set according to the nCounter Fusion Gene Analysis protocol, and the results were analyzed on the nSolver software.

Results: Of the 17 cases with known fusions, the NanoString assay confirmed the results in 10 cases, including 3 of 4 synovial sarcomas, 3 of 5 Ewing sarcomas and 2 of 2 myxoid liposarcomas. The assay was negative in 5 cases positive by FISH (two *FUS-CREB3L2,* two *EWSR1-FLI1*, one *EWSR1-ATF1*), and gave a different fusion result in 2 cases (*BCOR-CCNB3* in a synovial sarcoma, and multiple fusions in a myoepithelioma). Of the 17 cases with no known fusions, the NanoString assay identified fusions in 4 cases (BCOR-CCNB3 in a case resembling myxoid liposarcoma, MYH9-USP6 in a nodular fasciitis, IRF2BP2-CDX1 in a myoepithelioma, and COL6A3-CSF1 in a tenosynovial giant cell tumor). No fusions were found in the remaining 13 cases.

Conclusions: The NanoString nCounter Fusion Gene Analysis assay has the potential to identify fusion genes in soft tissue tumors utilizing FFPE material from both resection and core biopsy specimens. Although fusions were not detected in five FISH-positive cases, this may be due to the lack of an appropriate probe targeting the specific exon-exon junction; RTPCR studies are needed to confirm this. We predict that expansion of the code-set with more comprehensive coverage of fusion variants will allow for the development of a sensitive assay for sarcoma fusion gene detection.

2031 Utility of a Pan Genomic Fusion Panel (1300 Genes) on a Next Generation Sequencing (NGS) Platform in Evaluation of Cancer

Alka Chaubey, Ravindra Kolhe, Lisa C Watson, Deepa Jagdale, Claire Attwooll, WonSok Lee, Ashis K Mondal, Sadanand Fulzele. Georgia Regents University, Augusta, GA; Greenwood Genetic Center, Greenwood, SC; Illumina, Inc, San Diego, CA.

Background: Identification of novel gene fusions in malignancies can provide substantial tumor-specific information for research, & shows potential for diagnostic and targeted treatment purposes. Even though florescence in situ hybridization (FISH) is the current gold standard in fusion detection, it is limited in the number of genes it can detect in parallel. Similarly qPCR technique is also restricted by the same limitation and both lack high-resolution molecular characterization which is crucial for understanding the identity of these fusion partners. In contrast, RNA sequencing (RNA-Seq) is a powerful approach for simultaneous discovery of all possible fusion junctions in a single reaction. As oncogenes can fuse to multiple partners, the major advantage of using RNA-Seq technology is the ability to accurately identify fusions of all genes in the panel in a single sequencing assay, even without prior knowledge of fusion partners or breakpoints. In the current study, we assess the potential of an RNA-Seq capture panel consisting of 1300 fusion and cancer-associated genes, for identifying new gene fusions in different malignancies.

Design: RNA sequencing was performed on RNA isolated from FFPE blocks/cells lines on a NGS platform fusion calls were read and interpreted on the software provided by the manufacture (MiSeq, Illumina).

Results: We demonstrate robust detection of well-characterized cancer gene fusions using as little as 10 ng of RNA from commercially available cancer cell lines, such as BCR-ABL translocation detected in K-562 cells, and MLL-MLLT3 detected in THP-1 cells (acute monocytic leukemia). Furthermore, we show quantitative determination of gene expression levels with high reproducibility and high correlation to results obtained by whole-transcriptome RNA-Seq methods (R2 = 0.95 for ~1300 targeted genes). Similar results were achieved in sarcoma and hematologic malignancies. The results were compared with conventional FISH studies and karyotyping.

Conclusions: Here for the first time we describe an approach for selective enrichment of cancer-associated genes from RNA-Seq libraries that requires only a fraction of the sequencing depth and enables simultaneous fusion detection and expression profiling of over 1300 cancer-associated genes. We anticipate that this approach of obtaining high-resolution RNA-Seq data from FFPE/fresh specimens at reduced sequencing cost will facilitate studies of varied malignances which was not previously possible.

2032 The Intraoperative Immunohistochemical Staining of CD56 and CK19 Improves Surgical Decision for Thyroid Follicular Lesions

Sung-eun Choi, Eunah Shin, Ju Yeon Pyo, Soon Won Hong. Yonsei University Gangnam Severance Hospital, Seoul, Republic of Korea; Hanyang University Guri Hospital, Seoul, Republic of Korea; Gangnam CHA Hospital, Seoul, Republic of Korea.

Background: When a differential diagnosis is difficult in the thyroid follicular lesions with overlapping histological features, the immunohistochemical staining can help confirm the diagnosis. We aimed to evaluate the effectiveness of rapid immunohistochemical stains of CD56 and CK19 on frozen sections of thyroid follicular lesion and explore the possible gains and limitations of the practice.

Design: 86 nodules of 79 patients whose intraoperative frozen sections were not subject to IHC stains at all were selected as control group and 54 nodules of 50 patients whose intraoperative frozen sections could be subject to IHC stains if necessary were selected as study group. Nodules of the control group were intraoperatively diagnosed based on the H&E findings alone and the turnaround time(TAT) was recorded. Nodules of the study group were subject to IHC stains for CD56 and CK19 only when the cytological features were suspicious for PTC but the diagnosis could not be reached on H&E findings alone. PTC was diagnosed when the suspicious cells were CD56-negative and CK19-positive. When the suspicious cells were CD56-positive, the diagnosis of either follicular neoplasm or adenomatous hyperplasia was reached.

Results: The average TAT of the control group was 24 minutes. For the study group, the average TAT was 54 minutes. As for the type of intraoperative diagnosis, 5 out of 86 cases(6%) in the control group were diagnosed as follicular neoplasm, and 6 cases(7%) were deferred. In contrast, 7 cases out of 54(13%) in the study group were diagnosed as follicular neoplasm, and none were deferred. With respect to the diagnostic discrepancy between the frozen diagnosis and the permanent diagnosis, 3 cases out of 75(4%) in the control group showed discrepancy in the diagnosis; one case was initially diagnosed as malignancy on the frozen section, and then as benign on the permanent section; and two cases were initially diagnosed as benign on the frozen sections, and then as malignancy on the permanent sections. None of the study group had discrepancy between the frozen and permanent diagnoses.

Conclusions: Intraoperative immunohistochemical stains significantly decrease the diagnostic discrepancy. Considering the adverse effects of indefinite frozen diagnosis or discrepancy with permanent diagnoses, the intraoperative immunohistochemical stain can help to provide guidance to surgical treatment.

2033 Whole Slide Digital Imaging and Analysis of a PD-L1 Immunohistochemical Assay Is Quantifiably Reproducible

Jarish Cohen, Sarah Bowman, Daniel E Roberts, Vighnesh Walavalkar, Laura Laszik, Zoltan Laszik. University of California, San Francisco, San Francisco, CA.

Background: Immunohistochemistry (IHC) is a powerful tool that can provide prognostic and predictive information. Recent clinical trials have shown efficacy of monoclonal antibodies (mAb) that block the interaction of programmed death ligand 1 (PD-L1) with its cognate receptor PD-1, leading to heightened immunity against cancer. Accordingly, there has been clinical interest in using IHC to assess PD-L1 expression on tumors. However, analysis of this kind has traditionally relied on an arbitrary scale for staining intensity and is limited to one or few microscopic fields, which lends to under-sampling. Therefore, it would be advantageous to utilize a method that quantifies PD-L1 expression by IHC in a reproducible manner.

Design: To determine whether PD-L1 staining intensity could be performed in a reproducible manner, formalin-fixed paraffin embedded tonsillar tissue containing carcinoma was chosen as test case for antibody validation. 24 pairs of consecutive unstained slides were cut into 4 mm sections. Sections were incubated with PD-L1 mAb, and immunoperodixase staining with a brown chromogen was performed. Slides were scanned with an Aperio whole slide digital image scanner. Digital images were analyzed with Definiens tissue imaging software for percentage area of high, medium, and low signal intensity. Linear regression analysis was performed using Prism software.

Results: Subjective microscopic evaluation demonstrated consistent strong PD-L1 membrane expression on carcinoma cells, and variable intermediate and low level expression on stromal and lymphoid tissue. PD-L1 staining demonstrated significant reproducibility on paired consecutive tissue slides when assessed for percentage area of high signal intensity (R2=0.23, p=0.02). However, statistical significance was not reached for percentage area of intermediate (R2=0.036, p=0.37) and low (R2=0.11, p=0.11) signal intensity.

Conclusions: PD-L1 IHC shows quantifiable and statistically reproducible staining on the highest signal intensity tissue, an area that contains the most biologically relevant cellular population. However, PD-L1 staining was not reproducible for the intermediate and low signal areas. These areas grossly corresponded to background or "noisy" staining, which is a common byproduct of IHC methodology. Using rapid quantifiable analysis in this manner can provide data of higher sophistication than current methods of semi-quantitation of IHC-stained tissue. This method also has wider applicability as a means to identify cellular subsets that express PD-L1 within the tumor microenvironment.

2034 Digital Multi-Colour CTC Detection

Anthony Cooney, Brendan Ffrench, Cathy D Spillane, Carmel Ruttle, Noreen Gleeson, Ciaran O'Riain, Richard Flavin, Michael F Gallagher, Cara Martin, Orla Sheils, Sharon O'Toole, John O'Leary. Trinity College Dublin, Dublin, Ireland; Coombe Women & Infants University Hospital, Dublin, Ireland; Dublin City University, Dublin, Ireland; St. James's Hospital, Dublin, Ireland.

Background: As metastasis causes the majority of cancer deaths, detection of circulating tumour cells (CTCs) in blood could prove vital in early diagnosis**.** The majority of CTC isolation methods are focused on epithelial markers for identification, e.g. EpCAM and

panCK. However, CTCs entering the vasculature undergo epithelial to mesenchymal transition (EMT), limiting the power of epithelial markers in their identification. This study aimed to overcome this limitation by combining histochemical and multi-marker immunofluorescence staining, with whole slide digital imaging for accurate CTC enumeration in cancer patients.
Design: A method for labelling and digitally imaging CTCs was designed and optimised, using cancer cell lines spiked into whole blood. Cells were isolated using the filtration based ScreenCell® Cyto devices. Filters were then mounted on slides, Giemsa stained and digitally imaged. The filters were next labelled with a fluorescent antibody panel, including the epithelial markers, EpCAM and panCK, the metastasis marker, HER3, and the white blood cell marker, CD45, and again digitally imaged. The digital histochemical and fluorescent images were then overlaid, allowing pathologists to observe morphology and cancer specific markers in one image stack. The optimised protocol was then used to assess patient samples.
Results: The optimised protocol detected MCF7 cells spiked into blood with 100% accuracy. MCF7 cells stained positively for EpCAM/panCK and HER3 and were CD45 negative. While the negative controls 59M ovarian cancer cells were negative for EpCAM/panCK, HER3 and CD45. Blood cells were easily differentiated from cancer cells due to their CD45 positivity and EpCAM/panCK and HER3 negativity. The optimised protocol successfully identified CTCs in patient samples, confirmed by a panel of pathologists.
Conclusions: This protocol has overcome the weaknesses in current CTC identification methods, by combining histochemical and immunofluorescence staining in an integrated digital image. Thus, allowing cancer specific biomarker assessment, e.g. HER3, along with morphological evaluation of CTCs. This protocol will in the future allow for improved diagnosis of cancer metastasis.

2035 Optimizing Metastatic Bone Biopsies for Genomic Testing in Precision Medicine

Joanna Cyrta, Marc Schiffman, Brian Sullivan, Chantal Pauli, Olivier Elemento, Andrea Sboner, Brian D Robinson, Himisha Beltran, Mark Rubin, Juan Miguel Mosquera. Weill Medical College of Cornell University, New York, NY.
Background: Obtaining high quality nucleic acids (DNA and RNA) for next generation sequencing (NGS) from bone biopsies may be challenging. We report our experience using blood clots (BC) collected during bone biopsy to perform NGS in a precision medicine setting.
Design: Bone biopsies were done under CT guidance using OnControl® drill. BC were aspirated from coring site with a 12G needle. Bone cores and/or BC were rapidly placed in plastic cryomolds, embedded in OCT and frozen in isopentane with dry ice. If bone and/or BC was sufficient, part was submitted for *in vitro* tumor organoid development. Remaining cores were processed for standard pathology. H&E sections of frozen tissue were reviewed by pathologists to evaluate tumor content and guide DNA extraction. A minimum of 225ng of DNA and 100ng of RNA was required for whole exome sequencing (WES) and RNA sequencing (RNAseq), performed on Illumina HiSeq2500 (2x100bp and 2x75bp respectively).
Results: We studied 45 consecutive metastatic bone core biopsies from 39 prostate cancer patients. All biopsies were diagnostic. BC were collected in 39 cases. DNA sufficient for WES was extracted from 31 samples. Table shows WES parameters (mean, [range]) for representative bone-only or BC-only samples.

	Bone	Blood clot
Tumor DNA purity (CLONET)	50% [18-72%], n=7	49% [10-77%], n=8
Average depth	77x [63-78x], n=8	81x [72-86x], n=8
Capture efficiency	84.7% [83-86.5%], n=8	84.4% [82.9-86.8%], n=8
Fraction of bp covered at ≥10x	92% [82-95%], n=7	91.5% [89-94%], n=8

RNAseq was performed on 19/45 samples, including 12 BC-only cases. Initial growth of *in vitro* tumor organoids was obtained from a subset of BC samples.
Conclusions: Blood clots collected during bone biopsy for metastatic disease represent valuable material for genomic testing. Preliminary data suggest they are also suitable for tumor organoid development. For Precision Cancer Care of patients with advanced disease, NGS is becoming critical for determining mutation spectrum, neoantigen status and constitutional germline alterations; this pilot study shows that it is feasible even with challenging samples.

2036 Label-Free Identification of Amyloid Deposits in Tissue Using Infrared Spectroscopic Imaging

Bennett Davidson, Maria M Picken, Michael Walsh. University of Illinois at Chicago, Chicago, IL; Loyola University Medical Center, Maywood, IL.
Background: The early detection and typing of amyloid deposits in tissue biopsies is critical, especially with the emergence of new treatment strategies. Current techniques require suspicion of amyloidosis which then requires a tissue section being stained with Congo Red and examined using either polarized light or fluorescent light with a TRITC filter. Here we present a potential novel approach, Infrared (IR) Spectroscopic imaging, to identify abnormal protein deposits in a label-free approach based on the inherent biochemistry of the tissue without the requirements for staining.
Design: FFPE tissues (colon, pancreas and lung, n=6) were collected from the Loyola University Medical Center and sectioned at 4 microns on to special IR slides. Serial sections stained with Congo Red were examined with a fluorescent microscope with a TRITC for the presence of amyloidosis and regions of interest identified. High resolution IR images were acquired and compared to the stained sections.
Results: IR images collected from a range of tissues demonstrated difference in IR absorbance at certain biochemical frequencies, that could highlight regions of amyloidosis from unstained tissue sections (Fig 1).

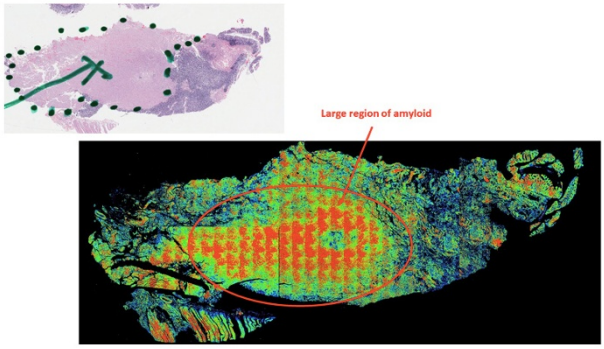

Figure 1. Color map of an IR image of the colon biopsy showed clear contrast correlating with the region of amyloidosis.

Furthermore, the amyloidosis was found to have a unique IR spectral signature compared to surrounding tissue (Fig 2).

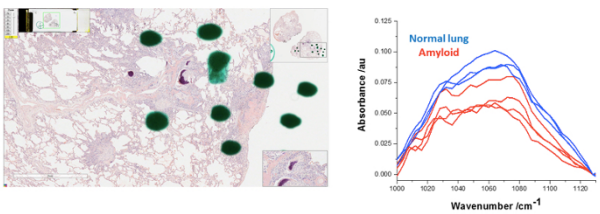

Figure 2. A lung biopsy with small regions of amyloidosis were identified from a H&E image by a pathologist (left panel, green dots were used to highlight areas of interest) and IR spectral signatures extracted from normal regions (blue) and amyloidosis regions (red). Even using a very short spectral range (1000-1120cm-1), clear spectral differences could be observed, demonstrating that amyloidosis has a unique spectral signature.

Conclusions: This preliminary study demonstrated that IR imaging represents a potentially useful approach to accurately identifying amyloidosis in tissues. Future work will focus on expanding the number of patients and the types of organs. We will also focus on determining whether we can subtype the amyloidosis class based on differences in the IR signature.

2037 Pathologic Staging of Endometrial Cancers: Is There Benefit to Submitting Adipose Tissue Remaining after Gross Identification of Lymph Nodes?

Nicola Dundas, Jordan Roberts, Ekene Okoye, Donna Coffey, Michael Deavers. Houston Methodist Hospital, Houston, TX.
Background: Accurate staging of cancer is essential for appropriate treatment. A critical component of staging is total lymph node (LN) count and the presence of cancer within these LNs. In an effort to maximize the number of LNs reported in cases of endometrial cancer, our department implemented a new policy, stating that after grossly identified LNs are submitted from LN dissection specimens, the residual adipose tissue is processed entirely. The purpose is to identify small LNs that are not seen on gross exam. The goal of this study is to evaluate the utility and clinical significance of this practice.
Design: We retrospectively reviewed cases of endometrial carcinoma in our hospital system over a year. The cases included endometrioid, serous, carcinosarcoma, mixed, and undifferentiated histologic subtypes. The reports were evaluated to determine the extent of LN dissection and the number of grossly identifiable LNs. The cases were divided into two groups: group 1 - traditional gross examination; group 2 - traditional gross examination and submission of residual tissue. Stage, extent of LN dissection, and lymphovascular invasion (LVI) were recorded.
Results: There were no significant differences between the groups with regard to stage, LVI, or the extent of LN dissection. Mean number of LNs identified and total positive LNs identified were not significantly different.

	LN only submitted	Entirely submitted	
	n = 52 cases	n = 36 cases	p
Stage I	34	23	
II	0	3	
III	14	6	
IV	4	4	0.1
LVI	18	12	1
Extent of LN dissection			
Pelvic	51	33	0.3
Aortic	28	14	0.2

	LN only submitted	Entirely Submitted	
	52 cases	36 cases	p
Avg LN/case	8.8	9.6	0.6
Cases with + LN	5	8	0.1
Total + LN identified	19	13	0.9
Avg # of positive LN (per + case)	2.4	2.6	0.8

Conclusions: Stage is one of the most important prognostic factors in endometrial carcinoma; it follows that surgical pathology practice should be optimized to accurately delineate the stage. After ensuring our groups did not differ with respect to important prognostic parameters, or to extent of surgical staging, we were able to show that LN yield does not significantly change with microscopic examination of grossly negative adipose tissue. Additionally, there is no significant change in the number of positive LNs identified with the change in procedure.

2038 SOX11 Expression In 125 Neuroendocrine Tumors: Increased Expression In Neuroendocrine Carcinomas

Laura P Fajardo, Gustavo C Verardino, Anabela C Caruso, Ana Lucia G Areas, Cesar S Bastos, Monique F Silva, Fabiane C Macedo, Nathalie QPC Correa, Roberta AP Albieri, Deborah P Siqueira, Andrea RC Pires. Fonte Medicina Diagnostica, Niteroi, RJ, Brazil; Universidade Federal Fluminense, Niteroi, RJ, Brazil; Hospital Naval Marcilio Dias, Rio de Janeiro, RJ, Brazil; Hospital Sao Vicente de Paulo, Rio de Janeiro, RJ, Brazil.

Background: SOX11 protein is a transcription factors acting in developing nervous system and tumorigenesis. It is detected by immunohistochemistry (IHC) in lymphomas (mantle cell, Burkitt and lymphoblastic), melanomas, and other tumors in humans. In lymphomas, SOX11 acts by downregulating PAX5, promoting plasmacytic differentiation. Several studies identified PAX5 frequent expression in atypical carcinoids and neuroendocrine carcinomas and tended to be negative in carcinoids, but there are no studies on SOX11 in these tumors.

Design: This study aims to evaluate SOX11 IHC expression in a tissue microarray (TMA) with 125 neuroendocrine tumors: 34 NET grade 1 (NET G1 / carcinoid tumors), 18 NET grade 2 (NET G2 / atypical carcinoid tumors), 65 neuroendocrine carcinomas (NEC) and 8 paragangliomas. SOX11 IHC nuclear expression was stratified by intensity (0 to 3+) and percentage of cells stained as focal (<10%), multifocal (10-50%) or diffuse (>50%).

Results: SOX11 expression was present in 34/65 of NEC (53,3%, most diffuse and strong; 27/51 small cell carcinoma, 1/3 large cell NEC, 3/3 Merkel and 3/8 MANEC), 4/18 of NET G2 (22,2%) and only one of 34 NET G1 (2,9%); none of paragangliomas were positive. There was also nuclear positivity in some endotelial cells, not yet described in humans.

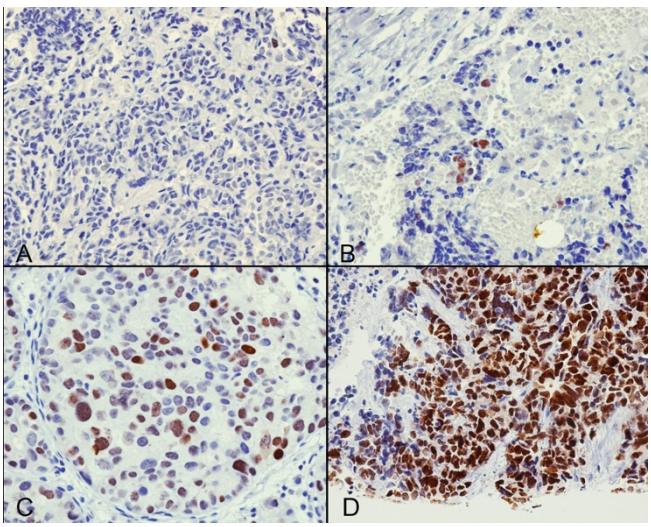

NEC SOX11 expression: (A) focal, 1+; (B) multifocal, 3+; (C) diffuse, 2+ and (D) diffuse, 3+; IHC, 40x.

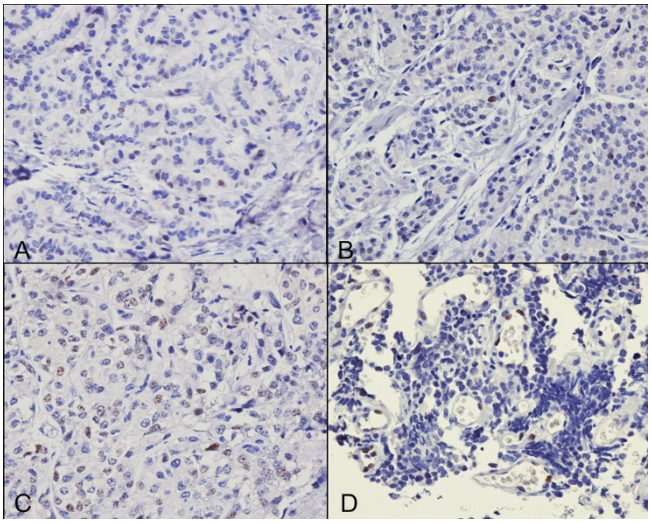

NET SOX11 expression: (A) NET G1, focal, 1+; (B) NET G2, focal, 1+; (C) NET G2, multifocal, 3+ and (D) endothelial cells; IHC, 40x.

Conclusions: The diffuse and strong expression of SOX11 in neuroendocrine carcinomas and mostly focal and weak in few NET G1 / carcinoid tumors and NET G2 / atypical carcinoid tumors proves that SOX11 is a useful marker for the diagnosis of NEC and discrimination between NET and NEC.

2039 Multiplex and Multispectral Analysis of Immune Cells in Tumor Draining Lymph Nodes of the Axilla in Breast Cancer

Syed Gilani, Chichung Wang, Clifford C Hoyt, Alejandro Contreras. University of Texas M.D. Anderson Cancer Center, Houston, TX; PerkinElmer, Inc., Hopkinton, MA.

Background: Lymph node status is an important prognostic factor in patients with a cancer diagnosis. In addition, host immune response has been shown to be involved in tumorigenesis, tumor progression, metastasis of the primary malignancy, and response to treatment. Thus, immune profiling of lymphocytes in axillary lymph nodes may provide additional insight into tumor biology and alterations important in the metastatic setting. Profiling of immune cells within lymph nodes using single antibody staining is important in predicting clinical outcome and multiplex analysis has shown differences in lymphocyte types between lymph nodes with and without metastatic carcinoma. However, the role and characterization of the immune cells within the tumor draining lymph nodes of positive or negative lymph nodes in non-treated and neoadjuvant treated patients, such as in the sentinel and nonsentinel lymph nodes of the axilla for breast cancer, have not been well characterized.

Design: Multiplex staining using antibodies against CD4 (Biogenex), CD8 (Leica), CD68 (Dako), PD-L1 (CST), cytokeratin (Dako), and Foxp3 with the Opal Multiplex Tissue Staining kit (PerkinElmer) was optimized on single, de-identified tissue sections (n = 4) of axillary lymph nodes with or without metastatic carcinoma in patients with or without neoadjuvant treatment. Multispectral analysis on the stained tissue sections was performed using VectraTM, a spectrally enabled whole-slide scanning system, followed by machine-learning-based automated image analysis using inFormTM software.

Results: Untreated lymph nodes stained simultaneously with CD4 (green), CD8 (yellow), CD68 (red), CK (cyan), Foxp3 (orange), PD-L1 (magenta), Dapi (blue).

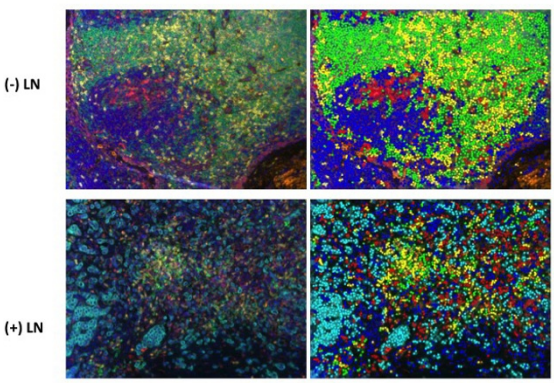

Conclusions: Phenotyping of immune cells immunohistochemical techniques has become a crucial source of information needed in the emerging field of cancer immunotherapy. We have successfully used multiplexed staining techniques and multispectral imaging analysis to analyze 6 markers simultaneously on positive and negative axillary lymph nodes from patients with breast cancer with or without neoadjuvant therapy. A large scale study is planned with quantitative and spatial analysis of these markers.

2040 In Situ Evaluation of Telomerase Expression and Function in Human Cells and Tissues

Nancy Greenland, Ajay Ravindranathan, Beth Cimini, Morgan Diolaiti, Bradley Stohr. University of California, San Francisco, CA.

Background: Despite the critical importance of the telomerase enzyme to cancer and aging, our understanding of its function and regulation has been hindered by difficulty in its detection. The catalytic subunit of the telomerase enzyme – the TERT protein – is typically expressed at very low levels. As a result, robust antibody detection of TERT protein and in situ hybridization detection of TERT mRNA in cells and tissues has proven extremely challenging. Furthermore, the levels of telomerase enzyme components do not always parallel the amount of functional enzyme in the cell.

Design: To address the challenge of in situ telomerase detection in cells and tissues, we validated RNAscope probes targeting TERT mRNA and the TER telomerase RNA subunit in human cell culture and two different tissues – testis and bladder. To enable simultaneous in situ evaluation of TERT mRNA levels and telomerase function in human cell culture, we combined RNAscope detection of TERT mRNA with our recently published in situ assay for telomerase function.

Results: The TERT and TER RNAscope probes demonstrate high specificity with very low background in cell culture models. In formalin-fixed human tissue, RNAscope probes enable detection of TERT mRNA and TER RNA in the expected cell types without the need for optimization of hybridization parameters. The resulting expression patterns highlight the importance of in situ detection. For example, our preliminary data indicate that within seminiferous tubules, TER RNA is most abundant in Sertoli cells while TERT mRNA is predominantly found in spermatogenic cells. Finally, by combining RNAscope detection of TERT with our recently described in situ assay for telomerase function, we demonstrate the ability to simultaneously measure TERT mRNA levels, telomere length, and telomerase function in individual cells of a heterogeneous cell culture population.

Conclusions: RNAscope probes provide sensitive and specific detection of TERT mRNA in human cell culture and tissues, despite the low level of TERT expression. Combining RNAscope TERT hybridization with our recently developed in situ assay for telomerase function provides what is, to our knowledge, the first assay to allow simultaneous evaluation of telomerase expression, telomere length, and telomerase function on a single cell basis. Together, these tools will enable new experimental approaches to dissect mechanisms of telomerase regulation in human cells and tissues.

2041 Is Mammary Analogue Secretory Carcinoma of the Salivary Glands a Distinct Entity from Acinic Cell Carcinoma: An Ultrastructural Study

Julie Guilmette, William C Faquin, G Petur Nielsen, Martin Selig, Vania Nose, Peter M Sadow. University of Montreal Medical Center, Montreal, QC, Canada; Massachusetts General Hospital and Harvard Medical School, Boston, MA.

Background: Mammary analogue secretory carcinoma (MASC) is a recently described neoplasm of salivary glands with a characteristic morphology complemented by a distinct immunohistochemical profile and specific cytogenetic translocation (12; 15) (q13; q25) resulting in an ETV6-NTRK3 gene rearrangement. Until this unique ancillary profile was reported, MASC was previously considered to be an acinic cell carcinoma (AciCC), either "zymogen poor" or intercalated cell predominant variant. Although immunophenotypic and cytogenetic features are diagnostically very useful, ultrastructural features can also provide important information about the relationship between MASC and AciCC.

Design: Following approval from the institutional review board, 6 cases of MASC were retrieved from the pathology files of the MGH. Electron microscopy was performed using formalin-fixed, paraffin-embedded tissue. Ultrastructural features of MASC were compared to those of classical AciCC.

Results: Ultrastructural examination of MASC revealed two cell populations. The first cell-type showed inter- and intracellular lumina lined with microvilli, some containing small secretory-like granules. While the second cell-type revealed a dilated endoplasmic reticulum with multiple mitochondria dispersed throughout the cytoplasm.

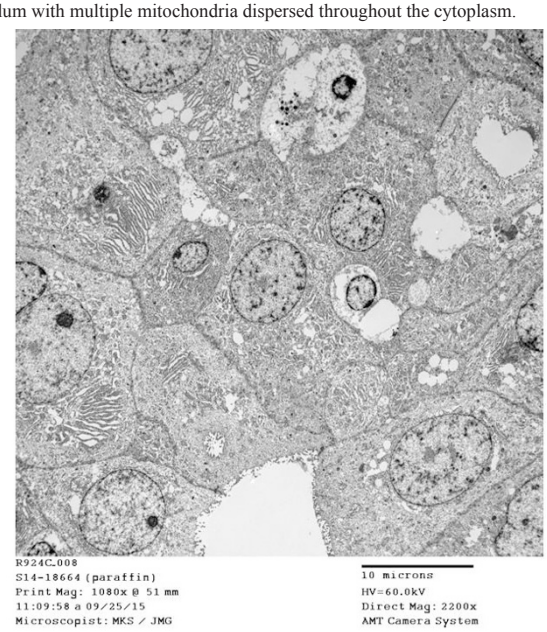

Similar to MASC, AciCC also showed two primary cell-types mimicking both acinar and intercalated duct cells of the parotid gland.

Conclusions: MASC and AciCC show significantly overlapping ultrastructural features. These findings suggest a very close proximity between these two tumors and suggest that MASC may be a peculiar variant rather than a separate entity from AciCC. Nonetheless, further studies are needed to elucidate the cellular origin and differentiation of MASC, and as more cases are reported, the actual outcomes data. Additionally, if unique molecular mechanisms drive two similar-appearing tumors, these differences might present opportune therapeutic targets for persistent or recurrent disease.

2042 Lymph Node Pooling. A Cost-Effective and Feasible Way of Lymph Node Molecular Staging in Colorectal Carcinoma

Laura Herrero, Iban Aldecoa, Natalia Rakislova, Carla Montironi, Nuria Planell, Pedro L Fernandez, Eva Fernandez, Salvadora Delgado, Dulce Momblan, Antonio Lacy, Antoni Castells, Miriam Cuatrecasas. Hospital Clinic, IDIBAPS, University of Barcelona, Barcelona, Spain; CIBERehd, IDIBAPS, University of Barcelona, Barcelona, Spain.

Background: The implementation of colorectal cancer (CRC) screening programs enable to detect the disease in early stages. In such scenario, an accurate diagnosis warrants the most appropriate treatment that can improve survival if implemented in initial stages. Nevertheless, up to 20% of stage II CRC patients recur from disease within 5 years of intended curative surgery. Molecular lymph node (LN) staging is far more sensitive and precise than pathological hematoxylin and eosin (H&E) staging. Besides, molecular detection of tumor burden in LN of CRC patients is associated with an increased risk of disease recurrence and poor survival. Yet, routine use of molecular LN testing is actually unfeasible due to the high amount of LN required for pathological CRC staging, its high costs and the time it requires. We aimed to propose an effective and efficient approach to LN molecular analysis for daily use in pathology departments.

Design: Tumor burden LN detection was performed with the reverse transcription loop-mediated isothermal amplification (RT-LAMP) for *CK19* mRNA. A total of 1.305 LN were harvested from 65 colectomy specimens. For each case, several LN were pooled together into PCR tubes up to a weight limit of 600 mg.

Results: A median of 2.5 tubes were obtained per case. Each tube held a median of 7.9 LN. Analysis of those 1.305 LN was performed in 164 assays, thus saving 87.5% of laboratory resources. An internal validation test performed with 42 cases showed equivalent results of the total amount of *CK19* mRNA copies/μL obtained from the analysis of each tube separately, and the analysis of the mixture of these different tubes in a single tube.

Conclusions: Lymph node pooling is a feasible and economic approach that reduces large numbers of molecular determinations. It enables the integration of molecular LN staging in daily pathology diagnosis of CRC patients, and allows a therapeutic management benefit.

2043 Agonal-Stress Vesicles Detected on Ultrastructural Examination in Pediatrics: Potential Mimicker of Metabolic Disease

John Hicks, Eric P Wartchow, Debra Keaney, Gary Mierau. Texas Children's Hospital and Baylor College of Medicine, Houston, TX; Children's Hospital Colorado, Aurora, CO.

Background: Acute or prolonged systemic failure, perinatal demise, or unexpected death in neonates and children often raise a concern for metabolic or mitochondrial diseases. With tissue obtained at autopsy or during intensive care period, workup for these disorders may be extensive and expensive. A potential pitfall is presence of cytoplasmic vacuoles within hepatocytes with microvesicular steatosis appearance. Microvesicular steatosis may indicate lipid metabolism or mitochondrial disorders. Ultrastructural examination is useful in identifying abnormal lipid accumulation, mitochondrial abnormalities, and metabolic/lysosomal diseases. Structures indicative of post-mortem agonal or pre-mortem stress have been termed agonal-stress (AS) vesicles. It has been implied that these vesicles contain acute phase reactants (APR) in response to cellular ischemia. This ultrastructural and immunohistochemical study explores APR nature of these structures.

Design: Archives at 2 pediatric hospitals were searched for cases with ultrastructural features of AS vesicles. 12 cases were identified with liver tissue submitted for routine processing and electron microscopy. Study population consisted of 6 males and 6 females) ages from 8d-6y) with medical conditions associated with ischemic stress. Immunohistochemistry for APRs was performed (c-reactive protein, fibrinogen, alpha-2-macroglobulin, alpha-1-antitrypsin, alpha-1-chymotrypsin).

Results: All routinely stained liver tissue sections shows variably-sized and numbers of vacuoles within hepatocytes, mimicking microvesicular steatosis. APR immunostaining highlighted the vacuoles with all antibodies, but was most intense with alpha-1-antitrypsin and alpha-1-chymotrypsin. Electron microscopy showed frequent vesicles with peripheral limiting membranes, containing finely granular to homogeneous content, sometimes resembling alpha-1-antitrypsin.

Conclusions: Agonal-stress vesicles are under recognized structures with routinely processed tissue and may be interpreted as microvesicular steatosis, leading to metabolic or mitochondrial disease workup. Prior to pursuing such a workup, electron microscopic examination may assist in identifying AS vesicles. Note that residual formalin-fixed tissue, frozen tissue and tissue recovered from paraffin blocks may be utilized for electron microscopy. Immunostaining for acute phase reactants in this study appears to confirm that agonal-stress vacuole contents are of an acute phase reactant nature.

2044 A Novel, Rapid, and Low Cost Method for Preparing Tissues with Metallic Stents for Routine Histology

Thom Jensen, Tyler A Jensen, Melissa Cessna, Dylan Miller. Intermountain Biorepository, Salt Lake City, UT; Intermountain Healthcare / University of Utah, Salt Lake City, UT.

Background: Endovascular stenting has become a common practice and cardiovascular specimens containing these metallic stents are frequently encountered in surgical pathology. Histologic examination of stented vessels is imperative, but special techniques are needed due to the presence of metal within the tissue. We describe a rapid and inexpensive method for preparing stented vascular specimens for routine histology.

Design: After formalin fixation and decalcification, stented vascular segments were placed in a plastic cylinder (boba tea straw) (Figure 1A). The cylinder was then filled with OCT embedding medium and placed in a -80º C freezer for 1 hour (Figure 1B). Using a handheld micro cutoff wheel tool (.040 in), the frozen cylinder was cut in ~1mm cross sections (Figure 1C). The sections were allowed to thaw and the stent strut shards removed with fine forceps (Figure 1D). The sections were then processed for routine histology.

Results: Histologic sections stained by H&E showed only minor tissue disruption around the stent struts (Figure E-F). The position of each strut could easily be determined, along with neointimal in-stent restenosis and (potentially) thrombosis. Local reaction to each strut could be surmised even if minor tissue disruption occurred. The entire process (from fresh tissue to glass slides) can be completed in 2-3 days (including fixation and decalcification). The incremental cost over that of routine histology is nominal (mainly the cut offwheel tool, approximately ~100 USD).

Conclusions: This method for examining stented vascular segments histologically could readily be applied in most pathology grossing rooms and serves as a highly practical solution to dilemma of examining stents histologically. While some tissue disruption may occur, the key histologic features relevant to stent pathology were preserved.

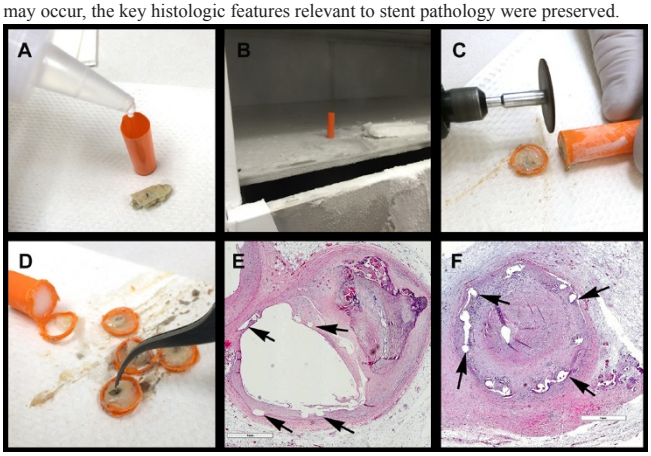

2045 Clear Cell Renal Cell Carcinomas with Clear Cell Tubulopapillary Renal Cell Carcinoma-Like Features: A Comparative Ultrastructural Study

Nuria Juanpere, Mercedes Simon, Ivonne Vazquez, Raquel Albero, Marta Salido, Anna Puiggros, Albert Frances, Laia Serrano, Sergio Serrano, Josep Lloreta. Hospital del Mar-PSMar, Barcelona, Spain; Pompeu Fabra University, Barcelona, Spain; Autonomous University of Barcelona, Barcelona, Spain.

Background: Clear cell tubulopapillary renal cell carcinoma (CCTPRCC) is recognized as a distinct entity. The differential diagnosis includes clear cell renal cell carcinoma (CCRCC) and papillary renal cell carcinoma (PRCC). CCTPRCCs are composed by tubules, papillae and nests lined by cells with clear cytoplasm and nuclei polarized to their luminal aspect. They have characteristic immunohistochemical and molecular profiles. Electron microscopy is very helpful in recognizing CCRCC and PRCC. However, there is limited information on the electron microscopic (EM) features of CCTPRCC. On the other hand, some CCRCCs have areas with light microscopic features very similar to CCTPRCC. Thus, the purpose of the present study has been to investigate the EM appearance of CCTPRCC and to compare it with similar areas in CCRCC.

Design: Five CCRCCs with CCTPRCC-like foci and one CCTPRCC are included in the present study. In CCRCCs, foci with CCTPRCC-like features were retrieved from paraffin blocks and fresh tumor tissue was available in 4 of them. CCTPRCC tissue was retrieved from paraffin. All samples were processed for electron microscopy and examined with a FEI CM100 electron microscope.

Results: CCTPRCC tumor cells contained mainly glycogen, either in pools or apparently within vesicles surrounded by a membrane. Lipid was not apparent. Nuclei were round, with loose chromatin and with the characteristic luminal polarization. Nucleoli were inconspicuous. The 5 CCRCCs with focal CCTPRCC-like areas were identified in a series of 87 CCRCCs (6%). In all the paraffin-embedded samples, tumor cells showed EM features very similar to those of the CCTPRCC case. In the randomly selected, glutaraldehyde-fixed samples, coalescing lipid droplets, glycogen pools and occasional membrane-bound glycogen were identified. Nuclei in these areas were often indented and had more conspicuous nucleoli.

Conclusions: CCTPRCC-like areas of CCRCC have EM features almost identical to CCTPRCC, while other areas in these tumors have conventional CCRCC EM findings. This could suggest that the two phenotypes reflect different metabolic profiles, and could be indicative of a sort of hybrid tumor.

2046 Comparison of 5 Methods for Extraction of Cell-Free DNA

Kevin Kelly, Vanessa Spotlow, Aleksandra Ras, Samantha Helm, Joan Malcolm, Gregory J Tsongalis. The Jackson Laboratory for Genomic Medicine, Farmington, CT; Dartmouth Hitchcock Medical Center and The Audrey and Theodor Geisel School of Medicine at Dartmouth, Lebanon, NH.

Background: Traditionally the detection of somatic mutations in a tumor of a cancer patient requires invasive tissue biopsies. However it has been discovered that cancer cells within these tissues routinely release pieces of DNA into the bloodstream where it is eventually excreted from the body. This small fragment of DNA that is not encapsulated within a cell has become known as cell-free DNA (cfDNA). The discovery of cfDNA brings about many possibilities for the development of liquid biopsy assays that can ultimately replace the traditional invasive biopsy with a simple blood drawn. To date one of the most common sources of cfDNA has come from plasma and there have been many efforts in trying to optimize the extraction and purification methods.

Design: In this experiment we evaluated and compared several commercially available extraction kits used to extract 24 plasma samples. These samples originated from patiets with non-small cell lung cancer, colorectal cancer, and pancreatic cancer, as well as, normal plasma. Samples were extracted following the recommended protocol provided by the supplier. Four different extraction methods were compared including magnetic bead mediated, silica bead based, vacuum column filtration, and standard column centrifugation. Samples were assessed for quality using the Nanodrop, Qubit, Bioanalyzer, and qPCR.

Results: The results showed that the magnetic bead based extraction method produced samples that had a greater quality as determined by the 260/280 ratio and yielded the highest total amount of DNA. Two different standard column centrifugation kits were assessed and one performed significantly better than the other yielding better purity and overall yield. The silica bead based method performed intermediately in all aspects but it should be noted that it was run using less starting material (0.75mL of plasma compared to the 1mL for the other methods) Lastly, the vacuum filtration method gave the poorest results.

Conclusions: While there are many different commercial kits for cfDNA extraction, our evaluation of 5 of the available kits resulted in the conclusion that some different extraction methods outperform others. Our data supports the use of magnetic bead based methods due to better overall yield, purity, and ease of use.

2047 Utility of Dual-Color Silver In Situ Hybridization and mRNA Chromogenic In Situ Hybridization in Adipocytic Tumor MDM2 Assessment

Jong T Kim, John D Reith, Wonwoo Shon. University of Florida, Gainesville, FL.

Background: MDM2 protein overexpression and gene amplification are present in virtually all atypical lipomatous tumors/well-differentiated liposarcomas (ALT/WDL) and dedifferentiated liposarcomas. Therefore, ancillary testing has been advocated to discriminate ALT/WDL and dedifferentiated liposarcoma from other adipocytic tumors in diagnostically challenging situations. Relatively recently, dual-color in situ hybridization (DISH) and mRNA chromogenic in situ hybridization (CISH) have been developed to detect *MDM2* gene amplification and mRNA expression, respectively. The purpose of this study is to test the effectiveness of these novel assays in diagnosing difficult adipocytic tumors.

Design: Formalin-fixed, paraffin-embedded sections from 5 ALT/WDL, 6 dedifferentiated liposarcomas, 4 pleomorphic liposarcomas, 3 myxoid/round cell liposarcomas, 12 conventional lipomas, 2 spindle cell lipomas, and 2 lipoblastomas were retrieved from our surgical pathology archives and examined by *MDM2*/CHR12 DISH (Ventana Medical systems, Tucson, AZ) and mRNA *MDM2* CISH (ACD Inc., Hayward, CA).

Results: By DISH, high-level *MDM2* gene amplification (>8 *MDM2*/CHR12 ratio) was present in all evaluated ALT/WDL and dedifferentiated liposarcomas. In contrast, none of pleomorphic liposarcoma, myxoid/round cell liposarcoma, conventional lipoma, spindle cell lipoma, and lipoblastoma demonstrated gene amplification. By CISH, all evaluated liposarcomas were also positive for *MDM2* mRNA expression, whereas lipomas and lipoblastomas were completely negative. In dedifferentiated liposarcomas, *MDM2* gene amplification and mRNA expression were observed in both well-differentiated and dedifferentiated components.

Conclusions: Similar to previous observations, this study confirms that both *MDM2*/CHR12 DISH and *MDM2* mRNA CISH can be useful in evaluating difficult adipocytic tumors and have the potential for routine application in surgical pathology practice. *MDM2* mRNA expression in pleomorphic and myxoid/round cell liposarcomas likely reflects other mechanisms of MDM2 activation without being amplified at the DNA level.

2048 Deep Convolutional Neural Network-Based Mitosis Detection in Invasive Carcinoma of Breast by Smartphone-Based Histologic Image Acquisition

Seokhwi Kim, Jungin Lee, Soohyun Hwang, Sooyoun Cho, Sangheum Hwang, Hyo-Eun Kim, Hyemin Shim, Miso Yang, Sangyong Song. Samsung Medical Center, Sungkyunkwan University School of Medicine, Seoul, Republic of Korea; Lunit Inc., Seoul, Republic of Korea; Seoul National University, Seoul, Republic of Korea.

Background: Mitosis counting is time and labor-consuming work and it frequently reveals inter-observer variability. Although deep convolutional neural network, the most accurate image classification algorithm, has been used for detecting mitosis, only public data sets were tested and it had never been utilized for routine histologic slide images. Recently, smartphone cameras with adaptors to the microscope were tried for easier image acquisition and they significantly resolved a barrier for applying computer algorithms to analyze histologic images.

Design: Histologic slides of 70 invasive ductal carcinomas of breast were selected and 1761 high-power field histologic images (400x) were acquired by using smartphone application with an adaptor attached to the microscope manufactured by us (Figure 1A). Mitoses were annotated by four pathologists blindly. More than three pathologists' concordance was regarded as true. 2004 mitotic cells and 801600 non-mitotic cells from 60 cases were divided into 10 sets and the algorithm was sequentially trained using fine-tuning method. After the training, ten patients' images were tested for the concordance of detection with pathologists.
Results: During the algorithm training, sensitivity for mitosis detection was calculated between 75-83%. Specificity for mitosis detection was increased to achieve 97% as we trained the algorithm with more images (Figure 1B). The trained algorithm identified 189 mitoses in 748 images from 10 cases and showed 79% sensitivity and 96% specificity for detecting mitosis compared to the pathologists. The detected mitoses were displayed in the application within 14 seconds in average (Figure 1C).

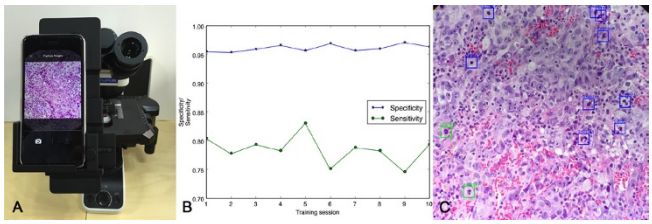

Conclusions: The proposed deep convolutional neural network-based mitosis detection system revealed remarkable sensitivity and specificity, and the performance improved as more images were utilized for training. Along with the smartphone application and the adaptor we manufactured, it assists pathologists to identify mitosis so that reduce time and labor costs, while resulting objective diagnosis.

2049 Feasibility of Ex-Vivo Confocal Fluorescence Microscopy for Rapid Evaluation of Tissues in Surgical Pathology Practice

Savitri Krishnamurthy, Andrea Cortes, Mirtha Lopez, Michael Wallace, Sharjeel Sabir, Gordon Mills, Kenna Shaw. MD Anderson Cancer Center, Houston, TX.
Background: Optical imaging techniques are currently available for imaging tissues without the need for any type of tissue preparation**.** We evaluated the feasibility of a confocal fluorescence microscopy (CFM) platform (Vivascope 2500, Caliber Inc. Rochester, NY) for examination of tissues encountered in surgical pathology practice.
Design: Tissues were obtained as fragments (0.5-1.0 cm) or 18 gauge core needle biopsies (CNBs) from surgical resections of lung, kidney and liver. The tissue was immersed in 0.6 mM acridine orange for 6 sec and imaged using a CFM platform at a wave length of 488 nm. Mosaics of the gray scale confocal images were studied at different magnifications to make a diagnosis of the tissue . The tissue was fixed in formalin to generate hematoxylin and eosin (H&E) stained tissue sections which were used for histopathological examination for categorization of the tissue as normal/benign or malignant. The sensitivity and specificity of the CFM platform for obtaining a tissue diagnosis was determined taking histological diagnosis as the gold standard.
Results: We imaged **47**tissue specimens (**39**tissue fragments; 18 lung,**13** kidney, 8 liver and **8** CNB: 4 kidney, 2 liver and **2** lung). Mosaics of gray scale confocal images of tissue fragments were obtained in 5-8 min. and CNBs in 3-5 min. The time taken for interpretation of tissue fragments ranged from 3 sec to 5 min (mean 43 sec) and that of CNB was 3 sec. The tissues were categorized as normal in 24 (**10** lung, **7** kidney and 7 liver) and as malignant in **23 (9** lung adenocarcinoma (AC), 2 squamous cell carcinoma (SCC);**7** renal cell carcinoma, 1 renal oncocytoma, **1 SCC** of renal pelvis; **3**AC in liver by histopathological examination. The diagnosis made on CFM images was concordant with H&E diagnosis in all the specimens of lung (**21/21**), kidney (**17/17**). While all 3 specimens of AC in liver were correctly identified on CFM images, 2 of the normal specimens of liver was incorrectly categorized as AC. The overall sensitivity and specificity of CFM for the assessment of normal parenchyma vs malignancy was 100% and 92% respectively.
Conclusions: 1. The ease and speed of acquisition of confocal fluorescence images of high quality together with the high sensitivity and specificity of diagnosis that can be made using the images suggests that CFM platform has an excellent potential for utilization in surgical pathology practice. 2. Prospective studies are warranted for establishment of CFM as a robust, reproducible and reliable platform for immediate assessment of tissues in surgical pathology practice.

2050 Inexpensive Improvements in Processing Techniques Can Significantly Improve Cell Block Cellular Yields

Kristin La Fortune, Melissa L Randolph, Harvey M Cramer. Indiana University Health, Indianapolis, IN.
Background: The ability to produce an adequate cell block profoundly impacts the diagnostic utility of cytology specimens. Cell blocks are routinely processed from fine needle aspirations (FNAs) or concentrated fluid samples, such as pleural and peritoneal fluids. Obtaining directed passes for the sole purpose of producing an adequate cell block is a common practice, particularly when the cytopathologist anticipates the need for ancillary immunocytochemical stains or molecular studies. It is especially disappointing when a highly cellular FNA yields a hypocellular cell block due to suboptimal processing in the laboratory. The purpose of this study was to develop an effective and inexpensive process for producing cell blocks that consistently yield abundant cellular material.
Design: Our institution developed a protocol for processing cell blocks that significantly improves the cellular yields. We assessed our failure rate, defined as having insufficient cellular material in a cell block for immunocytochemical stains or molecular studies, before and after implementing our protocol. The components of our new cell block processing protocol will be described in detail so that other cytology laboratories can benefit from this innovation.
Results: While refining our processing protocol, we identified several important factors that can dramatically impact the cellular yield of our cell blocks. One critical step is to prepare the specimen using a hemolytic fixative. We also utilized molds to control the depth of material within each cell block to prevent sectioning through cellular material. Our cell block failure rate over the two-year period prior to implementing our new procedure was 18%, which decreased to only 6% after implementing our new protocol in January 2015. This dramatic improvement in cell block yields was directly reflected in the marked decreased utilization of the cell transfer technique that we had been employing for immunostaining of cytology cases with inadequate cell blocks.
Conclusions: Our laboratory developed a protocol for producing cell blocks that consistently yields abundant cellular material, reducing cell block failure rates by two thirds. As the demand for molecular testing of cytology samples continues to increase, the need for adequate cell blocks becomes more pressing. Satisfying this demand in the era of precision medicine is indispensable if cytology is to maintain its clinical relevance.

2051 Development of RNAscope® 2.5 for RNA In Situ Hybridization on the Fully Automated Leica Biosystems' BOND Advanced Staining Platform

Henry G Lamparski, Bingqing Zhang, Melanie Miller, Thomas Laver, Casey Kernag, Daniel Kim, Keith Young, Kuang-Jung Chang, Nan Su, Xiao-Jun Ma, Yuling Luo. Advanced Cell Diagnostics, Hayward, CA.
Background: RNAscope® (Advanced Cell Diagnostics, Inc) uses a novel and proprietary method of *in situ* hybridization (ISH) to visualize single RNA molecules in a variety of sample types including formalin-fixed paraffin-embedded (FFPE) tissue. While the assay is routinely performed in a manual format, it is desirable to automate the assay to increase assay throughput as it applies to clinical diagnostic settings. Here we demonstrate the assay performance of RNAscope 2.5 reagents on a fully automated Leica BOND advanced staining system (Leica Biosystems).
Design: Using RNAscope's core technology, the RNAscope 2.5 reagents were optimized to perform on the fully automated Leica BOND platform incorporating a robust workflow. To evaluate repeatability and reproducibility of the RNAscope 2.5 assay on the automated Leica BOND platform, 3 lots of RNAscope 2.5 amplification/detection reagents were run on 4 Leica BOND RX instruments over 30 days using FFPE HeLa control slides stained for *dap*B (negative control) and Hs-*TBP* (positive control). In addition, using human FFPE tissues, clinically relevant biomarkers (high-risk-HPV, PD-L1) were tested to demonstrate performance of the RNAscope 2.5/Leica BOND platform for its use on real-world clinical specimens.
Results: Automation of the RNAscope assay on the Leica BOND platform resulted in a significant reduction in hands on-time. The optimized RNAscope 2.5 assay on the Leica BOND platform was demonstrated to be repeatable and reproducible on FFPE control slides when assessed for reagent lot-lot variation (n=3), instrument-instrument variation (n=4), intra-day (n=30 slides), and day-day performance over 30 days (n=5). There was strong and consistent staining (Leica BOND Brown and Red chromogens) with the probe *TBP* across all test conditions, with minimal to no background with the negative control probe *dapB*, thus demonstrating high signal-to-noise ratio.
Conclusions: Adaptation of the RNAscope 2.5 reagents to full automation on the Leica BOND platform was demonstrated to be highly repeatable and reproducible across multiple reagent lots, instruments, and days. The performance consistency and high throughput should allow for easy adoption into research and clinical settings. Evaluation of clinical relevant markers (HR-HPV and PD-L1) on relevant FFPE tissues is currently being tested and will be presented.

2052 Effects of Formalin Fixation Variables on DNA Integrity for Genomic Applications in Cancer

Martina Lefterova, Michael J Clark, Ravi K Alla, Shujun Luo, Massimo Morra, Elena Helman, Sean M Boyle, Scott Kirk, Parin Sripakdeevong, Mirian Karbelashvili, Deanna M Church, Michael P Snyder, John West, Richard Chen. Stanford University, Stanford, Ca.
Background: Formalin fixation and paraffin embedding (FFPE) is routinely used for tissue preservation. However, it leads to DNA fragmentation and mutation artifacts, which are exacerbated by variability of FFPE processing protocols. This impacts nucleic acid recovery for molecular diagnostics, particularly applications with high DNA requirements such as next-generation sequencing (NGS), and specimen types that are genetically heterogeneous such as tumors.
Design: To understand the role of formalin fixation on NGS-based somatic variant calling, we compared matched fresh frozen (FF) and FFPE samples from different sources on a clinical NGS cancer panel. First, we simulated different formalin fixation protocols on the NA12878 reference cell line, whose genomic profile is well characterized. We then tested seven clinical tumor FFPE samples with matched adjacent FF tissue. For all FF-FFPE pairs, we assessed raw DNA quality, library quality, sequencing metrics and variant concordance profiles.
Results: We observed a large degree of variability in DNA quality isolated from formalin-treated NA12878 cells. Processing temperatures >25C, fixation times >1day, and lack of buffering conditions led to severely fragmented extracted DNA and poor efficiency of library construction for an NGS cancer assay. Sequencing of damaged libraries led to decreased mapping to the reference assembly, high duplication rates, lower insert sizes, and lower base quality scores. Furthermore, higher rates of false positive and false negative "somatic" variant calls were observed in the formalin-compromised NA12878 relative to a fresh frozen sample. The majority of false positive calls were at allele frequencies <15% and represented increased deaminations (C>T and G>A). Assessment of mutational profile concordance in matched clinical FFPE and FF specimens is ongoing.

Conclusions: These results indicate that improper formalin fixation can severely impact the sensitivity and specificity of NGS-based tumor testing. In extreme cases, nucleic acids may not be recoverable, which can impact patient care as genomic assays are increasingly adopted in oncology to guide clinical management. Therefore there should be a concerted effort to optimize and standardize fixation protocols with regards to molecular diagnostic applications.

2053 Rapid, Inexpensive Slide-Free Histology via MUSE: Ultraviolet Surface Excitation Microscopy for Imaging Unsectioned Tissue

Richard Levenson, Zachary T Harmany, Alex R Krueger, Farzad Fereidouni. UC Davis Medical Center, Sacramento, CA; University of California Davis, Davis, CA.

Background: Widely used methods for preparing and viewing tissue specimens at microscopic resolution have not changed for over a century. They provide high-quality images but can involve time-frames of hours or even weeks, depending on logistics. Slide-free methods for rapid tissue histological analysis can cut hours off usual pathology slide preparation procedures, and can reduce cost.

Design: MUSE (microscopy with UV surface excitation) exploits the shallow penetration of UV light to excite only the most superficial tissue elements. The cut surface of otherwise unsectioned tissues can be stained within seconds to provide familiar contrast. The method is non-destructive, and eliminates requirement for conventional histology processing, formalin fixation, paraffin-embedding, or thin-sectioning. It requires no lasers, confocal, multiphoton or optical coherence tomography optics.

Results: MUSE samples from fresh (or fixed) tissues stained with general tissue stains such as eosin and DAPI, can generate high-resolution fluorescence images that can be converted in real time from fluorescence to H&E-like brightfield appearance for ease of interpretation. This sample-sparing method has potential to provide novel appreciation of cancer biology, to ensure availability of tissue from small biopsies for downstream analyses, and to enable histology and pathology in low-resource environments. Both familiar and novel contrast mechanisms are available, and some tissue components can be more easily visualized using MUSE compatible stains than with H&E, bypassing the need for additional special stains. Topographical information from portions of the sample below the cut surface can yield additional insights.

Conclusions: We have developed a new form of optical microscopy that generates diagnostic-quality histological images, with enhanced content, from fresh or fixed, but unsectioned tissue, rapidly, with high resolution, simply and inexpensively. We anticipate that there could be widespread adoption in research facilities, hospital-based and stand-alone clinical settings, in local or regional pathology labs, as well as in low resource environments

2054 Optimization of Rapid Immunohistochemical Stains on Frozen Tissue Sections

Haiyan Liu, Song Q Zhao, Yonghua Zhang, Zhiqing Zhang, Fan Lin. Geisinger Medical Center, Danville, PA; St. Mary's Hospital, Madison, WI; NovoDiax, Inc., Hayward, CA.

Background: Intraoperative frozen section (FS) consultation plays an important role in patient management. However, accurate diagnosis can sometimes be challenging. The application of rapid immunohistochemistry (IHC) on FS, recently introduced by NovoDiax, Inc. (Hayward, CA), can be useful when working on a difficult case. The aim of this study was to test and optimize the staining conditions for this rapid IHC technique using horseradish
peroxidase (HRP) polymer labeled mouse anti-human AE1/AE3 antibody.

Design: Fresh FS of the colon (N=3) and fallopian tube (N=2) were used to evaluate and optimize the ihcDirect™ Anti Pan-Cytokeratin Kit (Clone AE1/AE3) under various conditions as summarized in Table 1. A total of 30 protocols/combinations was generated from Table 1 and tested on the 3 colon and 2 fallopian tube samples. The optimal staining protocol, defined as the least performance time with appropriate staining signals and well-preserved histomorphology, was determined.

Table 1. Summary of Staining Conditions

Fixative	Fixation Time	Incubation Time	Temperature
1. Cold acetone 2. Frozen section fixative solution*	1. 30 seconds 2. 1 minute 3. 2 minutes	1. 3 minutes 2. 5 minutes 3. 10 minutes	1. Room (22°C) 2. 30°C 3. 37°C
Note: 25 ml of glacial acetic acid, 100 ml of 37% formaldahyde, and 375 ml of methyl alcohol			

Results: 1) Cold acetone was a better fixative than the frozen section fixative solution; 2) there were no significant differences among the three fixation times; 3) prolonged antibody incubation time such as 10 minutes yielded slightly stronger signals and background staining; in contrast, 3-minute antibody incubation provided adequate staining signals with no background staining; 4) no staining or only weak staining was observed when the IHC assay was conducted at 22° with 3-minute antibody incubation; in contrast, much stronger staining signals can be obtained at 30^{0}C. When raising the temperature to 37^{0}C, tissue preservation was poor.

Conclusions: The application of IHC on FS is practical and can be completed within 10 minutes. The optimal staining protocol for ihcDirect™ Anti Pan-Cytokeratin Kit (Clone AE1/AE3) is 1) fixed FS in cold acetone for 30 seconds; 2) incubated with the antibody for 3 minutes; and 3) IHC assay performed at 30^{0}C.

Further testing on various fresh frozen tissues with a variety of antibodies is needed before utilizing this new IHC method for patient care.

2055 Neuroendocrine and Non-Neuroendocrine Synaptophysin Expression in Prostatic Adenocarcinoma: An Immunohistochemical, qRT-PCR, and Ultrastructural Study

Josep Lloreta, Nuria Juanpere, Silvia Hernandez, Alba Font, Marta Lorenzo, Lluis Fumado, Jose A Lorente, Ivonne Vazquez, Raquel Albero, Laia Serrano, Sergio Serrano. Hospital del Mar-PSMar, Barcelona, Spain; Pompeu Fabra University, Barcelona, Spain; Autonomous University of Barcelona, Barcelona, Spain; Hospital Quirón, Barcelona, Spain.

Background: Non-neuroendocrine synaptophysin (SYP) expression is found in adrenal adenomas, in which it localizes in smooth endoplasmic reticulum and mitochondria but is not contained in neurosecretory granules. We identified diffuse SYP expression without other neuroendocrine (NE) markers in some prostate adenocarcinomas (PCa). The aims of the present study have been to confirm this finding by qRT-PCR and electron microscopy (EM), and to assess its prevalence as well as its relationship with tumor grade and progression in PCa.

Design: 100 radical prostatectomies with PCa were included in 4 TMA blocs. Immunohistochemistry for SYP (MRQ-40), Chromogranin A (CHROM) (LK2H10), and CD56 (MRQ-42) (Ventana-Roche, Tucson, AZ, USA) was performed. qRT-PCR for *SYP* (Applied Biosystems, Foster City, CA, USA) was performed in an independent series of 60 PCa and in 3 benign prostatic tissues (Parc de Salut MAR Biobank, Barcelona, Spain), with an overexpression cut-off of 2^(-DDCt) >2. A subset of 16 cases, including 4 with true NE differentiation, was processed for EM.

Results: Cytoplasmic SYP expression, with negative CHROM and CD56, was identified in 60% of PCa. It was strong in 13, moderate in 21, and weak in 26 cases. No dense core NE granules or vesicles were found by EM in any of the PCa with SYP expression alone. NE granules were identified in the 4 cases with true NE cells. SYP expression was more intense in tumors with Gleason score (GS) ≥7 (p=0.0006). In addition, *SYP* overexpression was detected by qRT-PCR in 8 out of 44 (18.2%) GS≤7 and in 5 out of 11 (31.3%) GS≥8 PCa (p=0.303). Clinical follow-up was available in 89 patients. No significant association between SYP expression and tumor progression was found.

Conclusions: Intense and widespread non-NE synaptophysin expression is a frequent finding in PCa, more often in high-grade tumors. Electron microscopy is recommended to rule out true neuroendocrine differentiation in these cases.

(FIS/Carlos III/FEDER. Grant PI12/01426, Spanish Ministry of Health).

2056 Validation of Multiplex Immunofluorescence Assays for Use in Analysis of Tumour Infiltrating Lymphocytes

James Mansfield, Henry Galletta, Richard Byers, Kenneth Oguejiofor. University of Manchester, Manchester, United Kingdom; PerkinElmer, Inc., Hopkinton, MA.

Background: Multiplexed immunohistochemistry (IHC) has the potential to improve conventional IHC staining allowing for analysis of multiple cell phenotypes while maintaining spatial context. Automated multispectral image analysis and computer-based cell recognition make the process more attainable, but stringent validation of multiplex IHC is still required. Pertinently, multiplex IHC allows for the characterisation and enumeration of immune cell densities in the tumour micro-environment, of particular importance for analysis of tumour-infiltrating immune cells which require multiple co-localised markers for their identification. In this study we systematically validated multiplex staining for a range of immune cell markers against single plex staining for each marker to determine the accuracy of the multiplex method.

Design: Validation of multiplex IHC was undertaken using a multi-tissue TMA stained in multiplex for CD3, CD4, CD56 and CD20 in a 4-marker validation and for CD3, CD4, CD8, CD20 and FOXP3 in a 5-marker validation. The TMA was composed of 72 cores including normal lung, pancreas, breast, prostate and stomach and malignant prostate, lung and colon. Spearman correlations measured agreement of immune cell populations with those of singly stained serial sections on a per-core basis. Single-stain/single-stain comparisons of corresponding immune cell populations provided baseline variation of immune cells in subsequent sections.

Results: All validation comparisons showed a highly significant correlation (P<0.0001), with strong correlation was observed between cores for the majority of multiplex stains. Specifically, for the 4-plex experiment, a high degree of correlation was observed for CD3, CD8 and CD20 with R^2 of 0.835, 0.950 and 0.870 respectively (P=<0.001); CD56 showed a lower degree of correlation between the multiplex and single stains with an R^2 of 0.584 (P=<0001). For the 5-plex experiment, a high degree of correlation was observed for high degree of correlation for CD3, CD8 and CD20 with R^2 of 0.87, 0.95 and 0.87 respectively (P<0.0001). FOXP3 showed a poor correlation of 0.74 and CD4 showed a poor correlation of 0.58 (P<0.0001).

Conclusions: Multiplex IHC is comparable to single stain IHC preserving precious samples and reagents while enhancing the information gained

2057 Immunoprofiling in Solid Tumors: Development of a 6-plex Imaging Assay To Characterize Infiltrating Immune Status in Solid Tumor Sections

James Mansfield, Kristin Roman, Chichung Wang, Junya Fujimoto, Ignacio I Wistuba, Jing Wang, Steven Lin, Clifford C Hoyt. PerkinElmer, Hopkinton, MA; MD Anderson, Houston, TX.

Background: Cancer immunobiology has grown exponentially recently. Immune cells clearly play a central, although sometimes conflicting, role in cancer. Obtaining phenotypic information about the various immune cells *in situ* is challenging. Existing methods can deliver phenotypic information on homogeneous samples (e.g., flow cytometry or RNAseq) or morphologic information in single stain IHC. We present a methodology for delivering quantitative per-cell marker expression and cellular phenotyping, analogous to flow cytometry, but from cells imaged *in situ* in FFPE biopsy sections.

Design: Twenty lung cancer sections and a lung cancer 84-core TMA were stained for CD3, CD8, CD68, CD137, FOXP3 and cytokeratin using a sequential multiplex IHC approach.

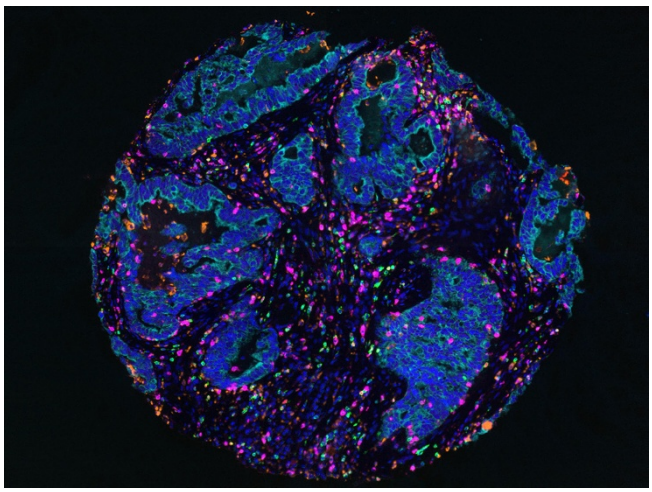

Slides were imaged using an automated multispectral microscope. Image analysis was performed to automatically quantitate phenotyped cells separately in the tumor compartment and in the stroma.

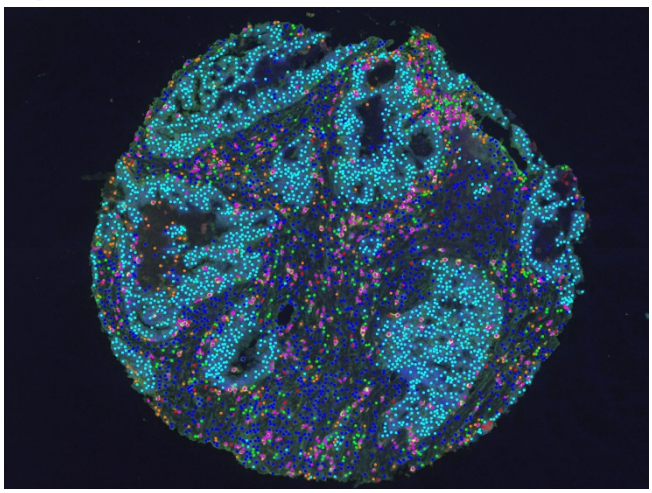

Results: An average of 20,759 cells were analyzed per section. The densities of phenotyped cells (counts/mm^2) for tumor and stroma were calculated, correlating well with manual assessments. *E.g.*, there were on average 9.9 Tregs/mm^2 in tumor (STD=21.1; min=0; max=97.4) and 107.1 Tregs/mm^2 in stromal tissue (STD=62.8; min=29.4; max=297.7). Counts were also obtained for CD3+, CD8+ and CD68+ cells. The expression of CD137 was analyzed for each phenotype of cell as well.
Conclusions: Development of assays to assess cancer-immune interactions in solid tumors is practical and within the capabilities of most research pathology laboratories. It is apparent in this study that immune activation or suppression can be characterized through cellular phenotype configurations in the tumor microenvironment. A range of configurations were observed and will be presented, demonstrating a capability of potentially great utility to the development of tumor immunotherapy agents.

2058 Scalable Next Generation Sequencing Workflow for Mutation Screening of Solid Tumors Using Ion S5XL Sequencer

Meenakshi Mehrotra, Dzifa Y Duose, Rajesh Singh, Bedia A Barkoh, Jawad Manekia, Jonathan Yau, Michael A Harmon, Mark Routbort, L Jeffrey Medeiros, Ignacio I Wistuba, Rajyalakshmi Luthra. The UT M.D. Anderson Cancer Center, Houston, TX.
Background: Detection of tumor-associated genomic mutations in tumors by next generation sequencing (NGS) involves complex workflow and relatively larger turnaround time (TAT) from sample preparation to data reporting. Multiple NGS platforms offer different workflows. Here, we compare the commercially available Ion torrent platforms (Ion PGM and Ion Proton) with new Ion S5XL NGS system for workflow, scalability, TAT and sequencing analysis.
Design: Eight solid tumor samples positive for various mutations as detected by prior sequencing using PGM and Proton were selected for study. Libraries were prepared using 10 ng of DNA from micro-dissected formalin-fixed paraffin-embedded (FFPE) solid tumor specimens using Ion AmpliSeq Library Kit 2.0 for comprehensive cancer panel (CCP 16000 amplicons), Oncomine comprehensive cancer panel (OCP 2530 amplicons) and cancer hotspot panelv2 (CHPV2 250 amplicons) as per manufacturer's instructions. The CHPV2 libraries were sequenced on PGM whereas the CCP and OCP libraries were sequenced on Proton. The libraries from different panels were multiplexed and sequenced on S5XL. 60pM pooled library was used for template preparation using Ion Chef and subsequently sequenced on S5XL using Ion 530 chip. Primary analysis was performed using Torrent Suite 4.6 software on board S5XL and secondary analysis using Ion Reporter. Assay performance characteristics such as sensitivity (using DLD1 cell line DNA) and reproducibility (using tumor DNA) were established for S5XL platform.
Results: A total of 108 variant calls (106 Single Nucleotide Variants and 2 indels) expected in the cohort were successfully detected by S5XL indicating complete concordance with other platforms. The average sequencing depth achieved for different panels using S5XL were 250X (CCP), 1250X (OCP) and 4500X (CHPV2). Ion chef automates the template preparation, enrichment and chip loading, hence simplifies the workflow. Availability of pre-made reagents for S5XL reduces the initialization time. Sequencing run time reduced from 4.5h to 2.5h with 3-5Gb output (between PGM and Proton) and 15-20 M mapable reads on 530 chip. Data analysis time (~ 2.5 h) is half compared to PGM and Proton. Lower limit detection of 5% allelic frequency was established along with high inter- and intra-run reproducibility.
Conclusions: In conclusion Ion S5XL system simplifies the workflow, showed the feasibility to run the smaller and larger panels on the same instrument with less TAT and good variant concordance with similar sensitivity and reproducibility as PGM and Proton.

2059 Centrosome Amplification (CA) and Mitotic Frequency Display Poor Concordance between Patient Tumors and Cancer Cells Cultured In Vivo: An Analysis of Breast, Pancreatic and Bladder Carcinoma

Karuna Mittal, Michelle D Reid, Angela Ogden, Da Hoon Choi, Meenakshi Gupta, Guilherme Cantuaria, Kristin Jonsdottir, Emiel AM Janssen, Beatrice Knudsen, Padmashree CG Rida, Ritu Aneja. Georgia State University, Atlanta, GA; Emory University, Atlanta, GA; West Georgia Hospital, Lagrange, GA; Northside Hospital Cancer Institute, Atlanta, GA, Georgia; Stavanger University Hospital, Stavanger, Norway; Cedars Sinai Medical Center, Los Angeles, CA.
Background: Amplified centrosomes and their corollary, aberrant mitotic figures are well recognized as beacons of malignancy. However, it has recently been brought to light that mitotic indices are much lower in patient tumors than continuously cultured cells, which may explain the clinical failure of many mitosis-targeted drugs that exhibited preclinical efficacy. We investigated the concordance between clinical tumor samples and cultured cancer cells by evaluating mitotic activity and CA.
Design: Using indirect immunofluorescence confocal imaging, we compared the number of mitotic figures (phosphohistone H3 staining) and CA (γ-tubulin staining), in paraffin-embedded clinical tumor samples of breast, pancreas and bladder (n=20 for each cancer type), immortalized cancer cell lines (MDA-MB-231-breast, Mia PaCa-pancreas and T24-bladder), tumor xenograft and patient derived cell line (breast).
Results: We found while <5% cells were mitotically active in clinical tumors, 5-15% of cultured cells were mitotically active. In contrast CA ranged from 35-50% in tumor samples and xenografts as opposed to 5-15% in continuous cell cultures. Patient-derived tumor cells displayed the highest CA (~50%), consonant with human tumors, albeit at low passage numbers only. Mechanistically, we found that hypoxia can induce CA and may explain the discordance between the extent of CA in patient tumors and cultured cancer cells. These findings were validated *in silico* by probing the publicly-available Kao microarray dataset using Gene Set Enrichment Analysis. Results suggested that high hypoxic breast tumors are enriched in CA and CIN-associated genes and also shows association to worse distant metastasis free survival.
Conclusions: These results bring to light the previously unrecognized variability in mitotic frequency and CA between various cancer model systems and highlight the importance of utilizing low-passage-number cell lines, preferably patient-derived, in the study of CA to more accurately represent cellular phenotypes in patient tumors.

2060 Front End Genomics: Using an Alternative Approach for the Recovery of High Quality DNA from Core Needle Biopsies

Wilfrido Mojica, Paul Mojica, Rama Dey-Rao, Don Sykes. University at Buffalo, Buffalo, NY; UCLA, Los Angeles, CA.
Background: The current pathology specimen-processing paradigm involves formalin fixation, paraffin embedding (FFPE) for optimal morphologic evaluation. This approach compromises nucleic acid integrity and recovery. Newer technologies applicable to clinical specimens, like sequencing and bioinformatics, have traditionally had to compensate for this compromised post-processed material. Developing a front-end procurement approach before FFPE would obviate the negative issues related to FFPE and deliver a better sample for these new technologies to work with. One area this approach could be applied to would be in the washing of core needle biopsies (CNB) where the intent of the wash is to recover the exfoliated cells. A comparative investigation assessing the qualitative and quantitative metrics of DNA between FFPE and unfixed, washed cells was undertaken.
Design: Four CNB were taken from 7 unfixed epithelial tumor cases. Two cores were immediately fixed in formalin and 2 washed with phosphate buffered saline. After processing, twenty-five 5 um thick sections were cut and the tissue curls retained in a microcentrifuge tube. The eluate from the washed CNB's was aliquoted into a portion dedicated for cytospin preparations and the other half for nucleic acid extraction. The recovered cellular and tissue material from each case was then processed using a commercially available DNA extraction kit (Zymo Research) and the samples subjected to quantitation by both nano-drop and Qubit assays. qPCR was performed using a commercial kit (Asuragen's Quantidex) to generate a QFI ™score that measures the absolute copy number of PCR-amplifiable DNA and functional quality of sample DNA. Finally, a portion of each sample was evaluated using the Agilent 2200 Tape Station System to determine the molecular weight (MW) of the recovered DNA and derive a DNA Integrity Number (DIN).
Results: Despite recovering more nucleic acids from the FFPE material relative to the wash specimens, the average number of functional DNA templates compatible with PCR amplification was greater in the latter than the former (8,042 vs. 6,496 copies).

The average QFI™ Score from these samples reflected this finding (102 (wash) vs 51 (FFPE)). The average MW of the DNA and DIN from the washes was 21 kilobases (kb) and 7.2 vs.13 kb and 6.5 for the FFPE samples.
Conclusions: A dedicated step prior to fixation can yield high quality DNA in sufficient amounts for molecular studies from CNB tissue. This approach allows the CNB tissue to be dedicated for morphologic and immunohistochemical analysis.

2061 Correlation of Flow Cytometry Analysis of Minimal Residual Disease (MRD) in Myeloma to Serum Free Light Chain (FLC) Nephelometry, Serum Protein Electrophoresis (SPEP) and Bone Marrow Chromogenic In Situ Hybridization (CISH)

Drew Nedved, Wei Cui, Mark T Cunningham, Da Zhang, Janet Woodroof. Kansas University Medical Center, Kansas City, KS.
Background: Follow-up of patients with myeloma to assess for MRD can provide prognostic value and impact treatment decisions. Laboratory assay of serum kappa and lambda FLC and SPEP offer a non-invasive technique for monitoring patients. Additionally, evaluation of bone marrow specimens for residual disease using kappa and lambda CISH and flow cytometry are increasingly used. We implemented a flow cytometry panel to assess for minimal residual neoplastic plasma cells in follow-up myeloma patients. Correlation of results has been undertaken between bone marrow flow cytometry and CISH, serum FLC assays and SPEP.
Design: The first fifty myeloma cases that had both flow cytometry and CISH studies were included in the study. Concurrent FLC assays and SPEP were performed according to standard methods. Flow cytometry data and bone marrow slides were re-reviewed in a blinded fashion. Neoplastic plasma cells gated with bright CD38/CD138 co-expression were identified based on clonality and aberrant antigen expression, with total cell count goal of 500,000 events. Back gates were also set up to look at the cytoplasmic kappa:lambda (k:λ) ratio in both the CD19 negative and CD45 negative subpopulations. Reference ranges for k:λ ratios and aberrant antigen expression were established using 40 normal marrows.
Results: Of fifty cases, six represented new diagnoses of multiple myeloma. All testing modalities correlated in these six cases. In the other cases (n=46), flow cytometry best correlated with CISH (94.0%). Three discordant cases showed <5% plasma cells, with positive flow cytometry subsets but negative CISH. SPEP detected a monoclonal paraprotein in all three cases, which were confirmed with immunosubtraction. Overall, the flow cytometry and SPEP had 74.5% correlation with six cases detecting a monoclonal protein spike but negative flow cytometry and another six cases showing positive flow cytometry and negative electrophoresis. Serum FLC nephelometry showed 79.6% correlation with CISH and 73.5% correlation with flow cytometry, with FLC normal in ten cases with positive MRD by flow cytometry.
Conclusions: This study emphasizes the need for multimodality follow-up of myeloma patients. The study showed a lack of sensitivity for detection of residual myeloma when using only serum FLC assays, and shows SPEP superior to FLC. Flow cytometry is a useful adjunct to detect minimal residual neoplastic plasma cell populations not otherwise detectable with serum FLC or CISH.

2062 EDTA–Based Decalcification of Bone and Bone Marrow- Ideal Tool for Protein and Nucleic Acid Preservation - A Pilot Study

Peter Ntiamoah, George H Ayob, Richard R Clarke, Doudja Nafa, Paulo A Salazar, Agnes Viale, Ahmet Dogan, Meera Hameed. Memorial Sloan Kettering Cancer Center, New York, NY.
Background: Bone and bone marrow biopsies are performed to diagnose diseases such as hematologic malignancies, primary bone tumors and metastatic tumors. In the era of increasing molecular testing for diagnosis and targeted therapeutics, preservation of nucleic acids and proteins are necessary and is required for the best patient care. For routine processing of bone specimens decalcification with inorganic acids (nitric acid or HCl) is used. Acid based methods allow fast turnaround times, but,, the procedure restricts use of the tissue for molecular diagnosis by damaging DNA, RNA and for some protein assays. To address this we undertook a pilot study using 10% EDTA decalcification solution, pH 7.2, as an alternate source for decalcification.
Design: Twenty formalin-fixed bone, bone marrows, and corresponding aspirate specimens were selected. For each specimen, one half was decalcified using acid-based method; the other half with 10% EDTA using Milestone's KOS Histostation at 37-45ºC. Decalcification time was between 8 and 24 hours, depending on sample type and thickness. Hematoxylin and Eosin sections were used to assess tissue quality and morphology. Selected samples were subjected to DNA/RNA extraction; tested for integrity of nucleic acids, and fluorescent in-situ hybridization (FISH) and next generation sequencing (NGS) assays. Immunohistochemistry (IHC) was performed on a subset of samples using a broad set of antibodies, including hematolymphoid markers.
Results: All acid decalcified tissues showed poor preservation of DNA and RNA on molecular and genetic testing by FISH and NGS assays; whereas EDTA-based samples showed very good results for DNA/RNA integrity, FISH, and NGS assays. The EDTA results were similar to that observed on fresh aspirates (Table 1). Results of IHC stains showed equivalent or better antigen preservation in EDTA decalcified specimens, compared to acid decalcified specimens.

Table 1: Comparison of fresh aspirate and biopsies decalcified by acid and EDTA shows that EDTA decalcification provides high DNA quality for most NGS assays comparable to fresh aspirates. In contrast, NGS assay are not possible with acid based decalcification.

	Sample	Read pairs examined	Mean target coverage	% target bases 30x
Case 1	Aspirate-fresh	29,174,336	1,299	99.00%
Case 2	Aspirate-fresh	37,296,917	1,633	99.09%
Case 3	Aspirate-fresh	34,443,717	1,420	99.10%
Case 4	Aspirate-fresh	30,188,471	1,310	99.07%
Case 1	Biopsy-acid	11,641,221	12	0.65%
Case 2	Biopsy-acid	4,940,352	3	0.10%
Case 3	Biopsy-acid	10,075,059	14	1.12%
Case 4	Biopsy-acid	12,924,007	19	5.55%
Case 1	Biopsy-EDTA	22,978,623	907	98.94%
Case 2	Biopsy- EDTA	15,900,564	601	98.55%

Conclusions: EDTA bone decalcification is practical and does not compromise turnaround time. There is good preservation of DNA, RNA and proteins; and applicable to routine IHC and a variety of molecular techniques including NGS and FISH assays.

2063 New Laser Based Imaging Approaches for Infrared Spectroscopy: Examples in Colon and Liver Tissue

Ramayee Periakaruppan, Vishal Varma, Hari Sreedhar, Francesca Gambacorta, Grace Guzman, Michael Walsh. University of Illinois Hospital and Health Sciences System, Chicago, IL.
Background: Infrared (IR) spectroscopic imaging is an emerging approach for tissue imaging and has the potential for adding additional biochemical information that can be of diagnostic or prognostic value without the need for dyes or stains. IR imaging has previously been limited to its feasibility in the pathology setting due to slow speed, requirement for extensive expertise and not being truly compatible with the current clinical workflow. New laser based imaging approaches, termed Quantum Cascade Lasers (QCL), are potentially revolutionary in now allowing for real-time biochemical imaging of tissue and providing instantaneous diagnoses back to the pathologist.
Design: We compared IR data collected from a traditional IR instrument and a new QCL based instrument and compared the two approaches using a colon tissue microarray and liver tissue microarrays of 50 patients providing ample cross sectional representation of a variety of diseases.
Results: Accurate automated segmentation between the major cell-types, disease states and diabetic status could be achieved using a separate validation classifier with a high degree of accuracy. In addition, the data could be acquired much faster and delivered to the pathologist in real-time. The new system was also demonstrated to be operational by a pathology resident who could identify regions of interest on the tissue in real-time and derive diagnoses.
Conclusions: New QCL based IR imaging approaches represent a huge advance in the applications of
label-free biochemical imaging for aiding pathologists in rendering a decision.
Here we show that the new technology can bring the advantages of traditional IR imaging to clinicians in a much faster and more clinically feasible approach.

2064 Predicting DNA Yield by Calculation of Extracted Tissue Area: Combining Digital and Molecular Pathology to Empower Genetic Testing

Mariana Petaccia de Macedo, Lauren E Haydu, Tiffany L Calderone, Khalida Wani, Sheila Duncan, Michael T Tetzlaff, Victor G Prieto, Michael A Davies, Jeffrey E Gershenwald, Alexander Lazar. MD Anderson Cancer Center, Houston, TX.
Background: Molecular pathology is widely used in cancer-care for predicting treatment response and giving prognostic or diagnostic information. Routine tests require the extraction of DNA/RNA from formalin-fixed paraffin embedded (FFPE) tissue. In order to spare limited tissues and maximize nucleotide yield for molecular assays, accurate prediction of the necessary amount of tumor is crucial. Here we present a model for systematic approach of extractions of nucleotides from FFPE samples and the results for the prediction formula for DNA yield obtained by extracted area.
Design: 203 primary melanoma FFPE samples were selected for integrative risk modeling projects at our institution. Blocks were retrieved from the melanoma bio-repository (MelCore). The proposed model consisted of selection of the best tumor area for nucleotide extraction from the initial H&E (Pre-DNA). 10-micron thick unstained slides were cut for manual microdissection and posterior DNA extraction (QIAamp FFPE-KIT®), followed by the confection of a final H&E (Post-DNA). The number of shears produced per case was rigorously annotated into MelCore database. Pre-and-Post-DNA H&E-slides were scanned with an Aperio-scanner®, and the microdissected area was measured using digital analysis (Aperio-Imagescope®). Mean microdissected tumor surface area was calculated by averaging measurements from each case's Pre-and-Post-DNA H&Es, and correlated to the resulting DNA yields measured by NanoDrop®.
Results: Median (range) Breslow thickness for the cohort was 3.0 (1.5-28.0) mm. From the 203 primary melanomas, the mean (range) tumor surface area (Pre-and-Post-DNA

scraped) and mean (range) number of 10-micron shears were 32.8 mm^2 (2.3-218.8) and 24 (2-92), respectively. The mean (range) of DNA in micrograms obtained per case was 7.4 (0.2-21.2). The mean (±SD) total nanograms of DNA per-mm^2 of a single 10-mm thick shear of scraped tumor tissue was of 24.0 ± 20.4 ng/mm^2 (median [IQR]: 20.2 [11.0-30.2]).

Conclusions: We describe an approach for processing FFPE samples in a molecular laboratory using digital pathology. In this cohort of primary melanoma, for each mm^2 surface area of a single 10-micron shear of tumor tissue, we retrieved a mean of 24.0ng of DNA. This metric can help planning and conduction of molecular assays. Although this approach was utilized for melanoma, it can be used as a starting point for validating formulas for any tumor type. Additional correlation is being made for the same samples considering pigmentation, tumor percentage and non-tumor content of each area, and also for RNA yields.

2065 Fluorescein: A Quick & Inexpensive Supplement to Frozen Section for Diagnosing Myometrial Invasion in Endometrial Cancer

Charles Quick, Kristin Zorn, Alexander Burnett. University of Arkansas for Medical Sciences, Little Rock, AR.

Background: Depth of myometrial invasion is an important determinant for performing lymphadenectomy in endometrial cancer. In some institutions, frozen sectioning at the time of hysterectomy is used to determine if lymphadenectomy should be performed. Frozen section analysis correlates with final pathology 87-92% of the time but is associated with increased time and expense. Additionally, gross assessment of areas of deep invasion may be difficult, leading to selection bias. We have observed that fluorescein labels normal myometrium and is non-fluorescent in endometrial carcinoma. We set forth to determine if fluorescein labeling could be a useful adjunct to gross and frozen section evaluation that can increase accuracy of operative staging.

Design: 15 women with endometrial cancer who were undergoing hysterectomy and BSO with possible lymphadenectomy were recruited for this study. Each patient was injected intravenously with fluorescein dye approximately five minutes prior to ligating the uterine arteries. After the hysterectomy was completed, the uterus was taken to pathology, sectioned and examined with a Wood's lamp to determine the areas of deepest invasion to submit for frozen sectioning. Specimen underwent frozen section of the most suspicious area determined by fluorescein evaluation and gross inspection, and these values were compared with the final pathology. Pearsons correlation coefficient was used to compare results between the groups.

Results: The correlation between depth of invasion predicted by fluorescein and final pathology was high with an r value of 0.8765 ($p<0.05$) and was comparable to the frozen section correlation with final pathology [r =0.8707 ($p<0.05$)]. When patients were categorized as either <50% or >50% invasion (a commonly used cut-off for nodal resection), Chi-square analysis revealed fluorescein to be significantly predictive of final pathology ($p=0.01$).

Conclusions: These results suggest that use of fluorescein labeling of the uterus can be used as a very rapid and inexpensive test that can help to determine the area of greatest invasion, thus aiding in identifying those patients who require lymphadenectomy for endometrial cancer.

2066 The Glazed, Erasable Tissue Sections. Disaccharides Protect FFPE Tissue Section Antigens from Air-Drying-Induced Masking and Allow Repeated Antibody Removal by Stripping

Susanna Ronchi, Giovanna Boi, Carla R Scalia, Rossella Gendusa, Giorgio Cattoretti. Universitá degli Studi di Milano-Bicocca, Via Cadore 48, 20900 Monza (IT), Italy; Azienda Ospedaliera San Gerardo, Via Pergolesi 33, 20900, Monza (IT), Italy.

Background: Drying of the tissue section, partial or total, during immunostaining negatively affects both the staining of tissue antigens and the ability to remove previously deposited antibody layers, in particular during sequential rounds of de-staining and re-staining for multiple antigens. The cause is a progressive loss of the protein-associated water, up to the removal of the non-freezable water, a step which abolishes the immunoavailability of the epitope. In order to describe and prevent these adverse effects, we tested, sugars, known to protect unicellular organisms from freezing and dehydration and to stabilize drugs and reagents in solid state form in medical devices.

Design: D-Lactose monohydrate, sucrose, glucose and galactose were tested on FFPE fully anonymous human material.

Results:

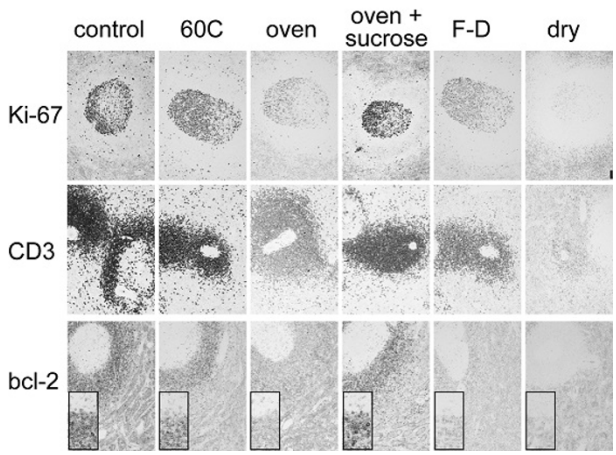

Figure 1 shows a series of staining conditions. Dewaxed, antigen-retrieved sections in distilled water were transferred to TBS as a control or air-dried in an oven at 60C for 1hr, rehydrated and immunostained for nuclear (Ki-67), cytoplasmic (bcl2) or membrane antigens (CD3). Air-drying invariably reduced the immunostaining intensity in a non-uniform manner to near complete loss. The effect was not dependent on the temperature, since keeping the section at 60C in distilled water for the same amount of time did not changed the immunoreactivity. Freeze-drying for 48h (during this process about 5% of the total water remains bound to the protein) reduced the immunoreactivity, but not abolished it.

Conclusions: Disaccharides (lactose, sucrose) prevented the air drying-induced antigen masking and protected tissue-bound antigens and antibodies from air-drying induced damage. Complete removal of the bound antibody layers by chemical stripping was permitted if lactose was present during air-drying. Lactose, sucrose and other disaccharides prevent air-drying artifacts, allow homogeneous consistent staining and the reuse of FFPE tissue sections for repeated immunostaining rounds by guaranteeing constant staining quality in suboptimal hydration conditions.

2067 Development of Multiplex Immunofluorescence Assays to Characterize the Tumor Microenvironment

Sandra Rost, Chenery Lowe, Cecile M Chalouni, Hartmut Koeppen. Genentech, South San Francisco, CA.

Background: Modulating the patient's immune system to treat cancer has shown clinical promise, however, predictive biomarkers need to be identified. The cellular composition of the tumor microenvironment (TME) is complex and evaluating multiple markers on a single slide is desirable in order to preserve tissue and to achieve recognition of spatial expression patterns. Multiplex immunofluorescence (m-IF) on formalin fixed paraffin embedded (FFPE) tissues can pose challenges such as autofluorescence, crosstalk or bleed-through. We report on the development of m-IF panels for simultaneous detection of up to 4 markers by systematically evaluating antibody (Ab) concentrations, detection systems and combinations of fluorophores.

Design: IF was performed on FFPE sections of melanoma and lung cancer using Alexa Fluor (AF)-conjugated primary Ab, unconjugated primary Ab followed by fluorescently labeled secondary Ab, or unconjugated primary Ab with polymer-based detection systems and tyramide signal amplification (TSA). Primary antibodies, fluorophores and panel composition are listed below. Detection of multiple markers using TSA required a sequential staining protocol with an elution step using antigen retrieval buffer between each staining. Staining was performed on a DAKO Autostainer Plus platform and stained slides were analyzed using a confocal microscope (Leica).

Results: Detection of specific staining was achieved with AF488, AF555 and AF647 in 3-plex panels, for 4-plex IF AF594 was added. The marker of highest abundance was detected with AF647, the marker of lowest abundance with AF594 or AF555. Expression of PD-L1 on MelanA- or cytokeratin-positive tumor cells was observed in sections of melanoma and lung cancer, respectively. PD-L1 expression was also seen on immune cells positive for CD3, CD8, CD68, CD163 or CD209. Bleed-through of strong signals into adjacent channels was avoided by minimizing amplification for detection of AF555 and AF594 signals.

	Marker 1 (AF647)	Marker 2 (AF488)	Marker 3 (AF555)	Marker 4 (AF594)
3plex	PD-L1[1]	MelanA[2]	CD68	
	PD-L1	CD68[3]	CD3[4]	
4plex	CD8[8]	CD68	CD3	PD-L1
	PD-L1	CD68	Cytokeratin[5]	CD209[7]
	PD-L1	MelanA or Cytokeratin	CD163[6]	CD209

[1]SP142, Spring Bio Science; [2]A103, DAKO, [3]KP1, DAKO; [4]SP34-2, Pharmingen; [5]5D3/LP34, Abcam; [6]10D6, Novus Biologicals; [7]h209, LSBio; [8]C8/144B, DAKO

Conclusions: We have developed m-IF panels that can be used on FFPE sections to visualize the immunophenotypic profile of the TME on a single slide. The goal is to determine the predictive value of such profiles for cancer immunotherapy approaches.

2068 Photoacoustic Mapping of Oxygen Saturation and Blood Volume in Ex Vivo Lymph Nodes of Colorectal-Cancer Patients

Emi Saegusa-Beecroft, Ashwin Sampathkumar, Eugene Yanagihara, Junji Machi, Ernest J Feleppa. University of Hawaii and Kuakini Medical Center, Honolulu, HI; Riverside Research, New York, NY.

Background: Imaging hemoglobin (Hb) oxygen saturation (SO_2) and blood volume (BV) may provide means of distinguishing between cancerous and non-cancerous tissue in lymph nodes (LNs). Current noninvasive techniques (MRI, PET) lack either spatial resolution or molecular sensitivity for Hb-SO_2 imaging. Photoacoustic (PA) imaging is a functional modality that images optical absorption contrast based on detection of ultrasound signals generated in tissues by the photoacoustic effect. This effect is the emission of acoustic waves that result from transient thermoelastic expansion when the incidental optical energy from a pulsed laser is absorbed and transformed into heat.

Design: In this study, PA imaging was applied to freshly-dissected LNs at wavelengths specific to oxygenated Hb (820 nm) and deoxygenated Hb (780 nm), and the corresponding PA-induced ultrasound was measured using a 26.2-MHz, f2 transducer. Volumetric maps of BV and SO_2 were obtained by 3D scanning.

Results: Of 10 colorectal LNs, 4 positive LNs demonstrated low (20 ± 12%) SO_2 and (24 ± 5%) BV levels. The remaining 6 negative LNs demonstrated higher (50 ± 10%) SO_2 and (40 ± 8%) BV levels.

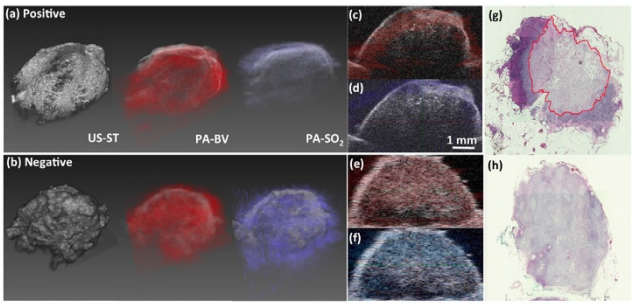

Figure 1 (a) and (b) show the volumetric reconstruction of the ultrasound (US) and superimposed photoacoustic (PA) data acquired on colorectal nodes that tested positive (g) and negative (h) for colorectal cancer, respectively. The structural (ST: gray), blood volume (BV: red), and oxygen saturation (SO_2: blue) metrics used for node classification is also shown in representative cross-sectional slices (c through f).

Conclusions: These results suggest that PA methods may provide real-time, intra-operative assessment of freshly-excised LNs from surgical specimens.

2069 TFE3 Immunohistochemistry: A Comparison of Two Methods, with Discussion of the Implications for the Diagnosis of TFE3-Rearranged Neoplasms

Rosalind Sandell, Allen M Gown, Andrew L Folpe. Mayo Clinic, Rochester, MN; PhenoPath Laboratories, Seattle, WA.

Background: *TFE3* rearrangement is characteristic of alveolar soft part sarcomas (ASPS), Xp11 translocation renal cell carcinomas (Xp11-RCC), and a subset of PEComas. Immunohistochemistry (IHC) for TFE3 has been considered a reliable surrogate for *TFE3* molecular studies, although data are limited. We compared 2 different methods for TFE3 IHC in 2 reference laboratories.

Design: Unstained sections from 98 consecutive archival cases plus 7 cases of ASPS were retrieved. Laboratory A: TFE3 (clone MRQ-37, prediluted, Ventana); HIER; Ventana Optiview detection system. Laboratory B: TFE3 (clone MRQ-37, 1:800, Ventana); HIER; Thermo Scientific Quanto detection system. Positive controls were normal human testis (Laboratory A) and Xp11-RCC (Laboratory B). Negative controls were employed. Scoring: "negative," "1+" (<10% positive), "2+" (10-50% positive), and "3+" (>50% positive).

Results: The 98 consecutive cases included 14 types of carcinoma, 13 undifferentiated pleomorphic sarcomas, 6 malignant melanomas, 5 solitary fibrous tumors, and 60 cases of 48 other tumor types. Laboratory A: 50 of 98 (51%) cases were TFE3-positive (1+: 9/50, 2+: 24/50, 3+: 17/50). Of the ASPS, 4 of 7 (57%) were TFE3-positive at Laboratory A (all 2-3+). Laboratory B: 5 of 98 (5%) cases were TFE3-positive (all 2+); these 5 cases were positive at both laboratories, and included a granular cell tumor, angiomatoid fibrous histiocytoma, leiomyosarcoma, metastatic pancreatic adenocarcinoma and mammary-type myofibroblastoma**.** Of the ASPS, 2 of 7 (29%) were TFE3-positive at Laboratory B (2+ and 3+); only 1 ASPS case was positive in both laboratories.

Conclusions: Despite using an identical mAb and similar methods / detection systems, we have found strikingly different results for TFE3 IHC in 2 different laboratories. We suspect that the most significant factor explaining these differences relates to the positive controls used for titration. Titration of the TFE3 mAb for optimal results on TFE3-overexpressing Xp11-RCC likely results in a test with higher specificity for TFE3-rearranged neoplasms, albeit with lower sensitivity, whereas titration to the physiologic TFE3 levels seen in testis and other normal tissues has the opposite effect. Ultimately, however, the results from both laboratories suggest that TFE3 IHC is an imperfect surrogate for *TFE3* FISH in the diagnosis of *TFE3*-rearranged neoplasms. FISH would appear to be the preferred technique for identifying rearrangements involving TFE3.

2070 Successful IHC Staining of Pancreatic Tissue after Optical Clearing for Advanced Imaging

Paul D Simonson, Ronnie Das, Eric J Seibel, Melissa P Upton. University of Washington, Seattle, WA.

Background: Novel imaging techniques are creating exciting possibilities for rapid, more complete characterization of patient tissue specimens via three-dimensional (3D) imaging. 3D imaging only enhances tissue characterization when it can construct a 3D tissue profile that is much thicker than the width of a normal histology tissue section (5 um). As light passes through tissue, it is scattered by particles or other index of refraction mismatches such that, past a certain point, high-resolution imaging is no longer possible. In order to combat this problem, special "optical clearing agents" have been developed, including FocusClear, which have improved imaging depth by an order of magnitude. While 3D imaging has the potential to give a much more complete characterization of tissue, it is essential that tissue be available for subsequent IHC analyses. Our aim was to compare IHC staining results of cleared and uncleared pancreatic tissue as an important step in our development of a rapid pancreatic biopsy 3D imaging device.

Design: Pancreatic tissue, including cancer and non-cancer specimens, was collected from 5 patients. Specimens were received in formalin and split into control and test samples, with the control placed in formalin and the test sample placed in FocusClear. The samples were incubated for times ranging from 2-15 hours, after which the test samples were rinsed extensively with phosphate-buffered saline, then placed in formalin. The specimens were subsequently submitted for standard tissue processing and stained with H&E, as well as immunohistochemically for CK7 and vimentin (markers for diagnosis and potential prognosis). The resulting slides were inspected visually and computationally by finding the mode of the intensities of the IHC-stained pixels using the *IHC Image Analysis Toolbox* and *ImageJ*.

Results: Blinded, side-by-side images of the IHC-stained test and control samples were presented for visual inspection by two pathologists who were unable to detect any difference in the staining qualities or intensities. Similarly, no significant difference in intensities was identified computationally using the approach outlined above.

Conclusions: For CK7 and vimentin IHC, no significant difference in staining quality or intensity was observed for optically-cleared versus control tissue, even for long incubation times. This result is an important step in the development of 3D imaging systems wherein the tissue retains reversibility and transferability to IHC, as previously demonstrated for brain tissues.

2071 Breast Biomarkers Can Be Reliably Tested on Tissue Fixed and Processed by Same Day Automated Microwave-Assisted Method

Elzbieta Slodkowska, Fang-I Lu, Wedad Hanna, Houman Nafisi, Guangming Han, Patrice Boulianne, Sharon Nofech-Mozes. Sunnybrook Health Sciences Centre, University of Toronto, Toronto, ON, Canada.

Background: Recommendations to validate any modification in breast cancer biomarker testing have been endorsed by CAP and other regulatory bodies to ensure accurate testing (Fitzgibbon et al 2010). Accordingly, any proposed modification has to be tested against a previously validated technique. For modifications in preanalytical variables this entails creating a validation set of paired samples, consisting of a combination of positive (P), low positive (LP, <10%) and negative (N) cases that have been prepared under the same conditions and differing only with respect to the modified variable. Microwave-assisted rapid tissue fixation and processing (MWARTFP) significantly reduces tissue processing time. Herein, we report our experience in validation of breast biomarkers using rapid method for tissue fixation and processing.

Design: A set of 62 breast cancer resection specimens (enriched for HER2+ cases) was prospectively selected for validation. Upon receipt from the OR, a core-sized sample of *fresh tissue* was aquired and immediately processed using a 2 hr protocol for MWARTFP (Pathos, Delta, Milestone). The remaining blocks were fixed for a minimum of 8 hours and processed by conventional overnight tissue processing (CTP). Parallel blocks from each case were placed on the same run on the immunostainer and read by the same pathologist.

Results: In all benign ducts immunoreactive cells for ER and PgR on MWARTFP were identified.

Biomarker	Status, CTP	Concordant	% Agreement
ER (SP1)	P (*LP*)	46(2)/48(4)	95.8 (50)
	N	14/14	100
PgR (1E2)	P (*LP*)	35(7)/35(7)	100 (100)
	N	27/27	100
HER2 IHC (4B5)	P	21/21	100
	N	29[2]/29	100
HER2 FISH[1]	Amplified	18/18	100
	Non-amplified	18/18	100
	Equivocal	1[3]/2	50

[1]fluorescent in situ hybridization (FISH)
[2]One CTP HER2 IHC 1+ scored 2+ on 2 hr protocol but wasn't amplified.
[3]One CTP ISH equivocal case scored negative on 2 hr protocol.

Conclusions: Hormone receptors and HER2 status tested on MWARTFP and CTP are highly concordant. Discrepancy between MWARTFP and CTP on cases with very low positive ER could be attributed to smaller surface area tested on the study cores compared with the clinical blocks. This technology can be applied in pathology labs to provide comprehensive and efficient service for rapid (same day) diagnostic units including reliable biomarkers testing.

2072 Ex Vivo Confocal Laser Endomicroscopy Is Useful in the Evaluation of Pancreatic Cystic Lesions

Benjamin J Swanson, Wendy Frankel, Darwin L Conwell, Peter Muscarella, Somashekar G Krishna. The Ohio State University Wexner Medical Center, Columbus, OH; Montefiore Medical Center, Bronx, NY.

Background: Confocal laser endomicroscopy (CLE) allows real-time imaging of mucosal and cystic surfaces. This technique has been utilized for in vivo endoscopic ultrasound guided (EUS)-needle based CLE evaluation (nCLE) of pancreatic cystic lesions (PCLs). While small PCLs can be entirely submitted for histologic analysis, large PCLs are more problematic and ideally would be selectively sampled during gross examination. Here, we study the utility of ex vivo CLE in the analysis of resected PCLs and correlate with both in vivo nCLE and direct biopsies.

Design: Seven (n=7) patients with PCLs initially underwent in vivo EUS-nCLE. All patients had surgical resection of their PCL. Resected PCLs underwent ex vivo CLE with direct biopsy of areas of interest. The remainder of the PCL was entirely submitted for histologic analysis.

Results: Thirty-three biopsy (n=33) specimens were obtained from the intracystic surface of seven resected PCLs. Final pathologic diagnoses were: intraductal papillary mucinous neoplasm (IPMN, n=2), mucinous cystic neoplasm (MCN, n=2), serous cystadenoma (SCA, n=1), cystic neuroendocrine tumor (cystic NET, n=1), and epidermoid cyst of accessory spleen (n=1). Representative images of in vivo, ex vivo and biopsies are shown in figure 1. IPMN cases showed characteristic villous structures that were observed by all 3 modalities. For MCN cases, a band of epithelium and characteristic 'ovarian stroma' was observed with more clarity in ex vivo imaging.

CLE images in cystic NET showed nests of cells which correlated with biopsies. The characteristic vascular network of SCA seen in CLE imaging was not observed in biopsies.

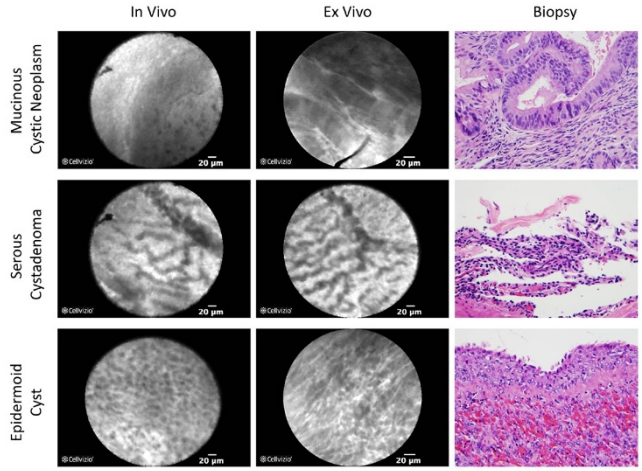

Conclusions: Ex vivo CLE images correlated with in vivo EUS-nCLE images as well as biopsies. These findings are encouraging for further delineation of CLE guided analysis of PCLs. Directed biopsies with CLE may help define features distinguishing low from high grade dysplasia in IPMN and MCN. Thus, future studies may allow selective sampling of large PCLs during gross examination.

2073 Correlation between Immunohistochemical BRAF V600E Expression and Mutational Status Detected by Two Different PCR Based Molecular Techniques in Papillary Thyroid Carcinomas

Jordi Temprana-Salvador, Javier Hernandez-Losa, Carles Zafon, Jessica Camacho, Sherley Diaz, Irma Ramos, Rosa Somoza, Ingrid Strohecker, Oscar Gonzalez, Amparo Garcia-Burillo, Santiago Ramon y Cajal, Carmela Iglesias. Vall d'Hebron University Hospital, Autonomous University of Barcelona, Barcelona, Spain.

Background: Thyroid cancer is the most common malignant endocrine neoplasia, and papillary thyroid carcinomas (PTCs) represent about 80% of these cases. **BRAF point mutation V600E is detected in over 50% of PTCs.** Clinical studies have shown an association between BRAF mutation and clinical progression, invasion, and recurrence in PTC. In this study we investigate the correlation between the **BRAF V600E mutation** and **BRAF V600E protein expression** in PTC patients.

Design: Immunohistochemistry (IHC) was utilized to analyze BRAF V600E protein expression (VE1 Ventana). Presence of the BRAF V600E mutation was determined in formalin-fixed, paraffin-embedded tissue (FFPE) by the **Cobas 4800 BRAF V600 Mutation Test** and by **EntroGen Thyroid Cancer Mutation Detection Kit**, which also assesses **KRAS**, **NRAS** and **HRAS** mutations. **38 cases** were included in our study: 33 PTCs (follicular variant: 4), and 5 follicular carcinomas as negative control.

Results: In PTC patients, IHC BRAF V600E expression was detected in 24/33(72.7%). The BRAF V600E mutation was observed by Cobas in 24/33(72.7%) and by EntroGen in 23/30 patients (76.7%)(3 patients were nonassessable). Follicular variant of PTC had V600E mutation in 2/4(50%) with perfect concordance between the 3 methods. Follicular carcinomas were WT by both molecular methods and also negative by IHC. The overall concordance rate between both molecular techniques was **96.7%(κ=0.911)**, between IHC and EntroGen was 96.7% (κ=0.911) and between IHC and Cobas was 93.9%(κ=0.847).

2 discordant cases were found. The first one showed BRAF V600E mutation by both molecular tests, however it did not show BRAF V600E expression by IHC. The second one showed BRAF V600E mutation by EntroGen Kit and BRAF V600E expression by IHC, but Cobas did not detect this mutation (<5% tumor in FFPE).

Additionally EntroGen Kit detected one HRAS mutation in 1 follicular carcinoma. No KRAS or NRAS mutations were observed.

Significant association was observed between BRAF V600E mutation and **presence of vascular invasion** (p=0.033). No differences were found in gender, multifocality, extra-thyroid extension or lymph node metastasis.

Conclusions: This study demonstrated a significant correlation between BRAF immunostaining and BRAF V600E mutation in PTC, which could be an important diagnostic tool improving PTC diagnosis. Both Cobas BRAFV600 and EntroGen Thryoid Cancer Mutation Detection Kit are useful to perform screening of BRAF mutation in Thyroid neoplasias. Moreover, EntroGen kit also assesses RAS mutations.

2074 Cell & Tissue Display (CTD): An Alternative Multipurpose Tool for Microscopy

Nicholas Theodosakis, Goran Micevic, Marcus W Bosenberg, Nemanja Rodic. Yale School of Medicine, New Haven, CT.

Background: Cultured cells and tissues are often used separately as controls in clinical diagnosis or research. Herein we describe a novel block making technique that can achieve multiplexing as well as fine spatial control of both cell lines and tissues within the same histologic block, giving a tissue microarray-like arrangement of specimens on a slide.

Design: To improve on existing methods for embedding cultured cells, we first developed an agarose mold-based homogenization and embedding protocol. We started by creating the first CTD array using dilutions of human melanoma cell lines. We also constructed a second CTD array of 16 mouse tissues (termed, "mouse 1") and an additional third array of 11 established human melanoma lines alongside a control normal human skin (termed, "melanoma 1).

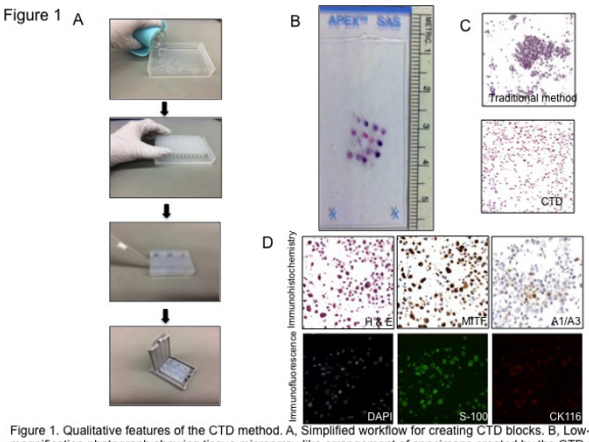

Figure 1. Qualitative features of the CTD method. A, Simplified workflow for creating CTD blocks. B, Low-magnification photograph showing tissue microarray-like arrangement of specimens created by the CTD method. C, High magnification photomicrograph showing show improved cellular homogeneity of the CTD method (lower panel) compared to the traditional method (upper panel). D, Preserved antigen detection following CTD block making using both IHC and IF assays.

Results: Using our first CTD array, we demonstrated improved homogeneity and more precise control of cell number across a 4-log range while preserving epitope antigenicity. Using our second array, "mouse 1", we achieved tissue fragment multiplexing and a fine level of spatial control as we successfully tiled 16 mouse tissues within a single histologic block. Finally, using our "melanoma 1" array, we demonstrated that multiplexing of both multiple cell lines and tissue fragments can also be achieved within the same histologic block.

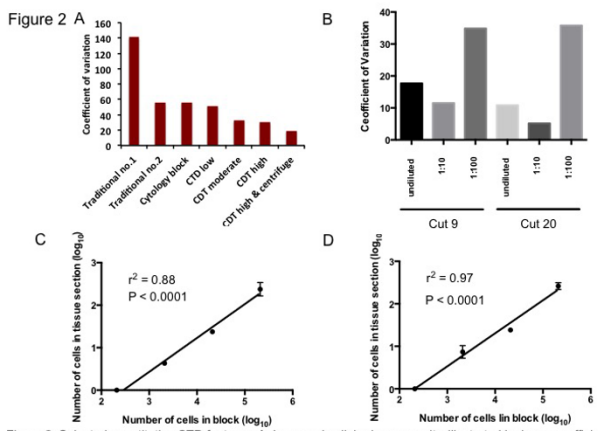

Figure 2. Selected quantitative CTD features. A. Improved cellular homogeneity, illustrated by lower coefficient of variation of intercellular distances, *d*, for several iterations of CTD histologic blocks. B, Improved cellular homogeneity amongst serial sections within the same CTD block. C&D. Concordance between the number of cells deposited into a CTD block and visible cells in final slide sections; cuts 9 and 20, respectively.

Conclusions: CTD is an alternative method for histologic block making that achieves novel features such as reduced variability amongst serial cuts as well as multiplexing of cultured cells and tissue fragments.

2075 Cytology Waste or Molecular Treasure? A Proposed Algorithm for Molecular-Oriented Cytology Specimen Utilization

Shaozhou Tian, Maria E Arcila, Andre Moreira, Justyna Sadowska, Sumit Middha, Oscar Lin. Memorial Sloan Kettering Cancer Center, New York City, NY.

Background: Molecular testing is increasingly used in the management of patients with cancer. This is frequently performed on material obtained from minimally invasive biopsies, either by core or fine needle aspiration (FNA). The use of FNA specimens is traditionally limited by the quantity of available material for higher demand assays such as Next Generation Sequencing (NGS). We have developed and validated an integrated approach of molecular testing using FNA biopsy processing waste that was not previously used for diagnostic purposes and discarded. This material includes post centrifugation supernatant and residual material from needle rinses. This process drastically improves DNA recovery while minimizing material exhaustion.

Design: Forty-eight positive sequential cytology cases, with at least 10% tumor, were collected. Cell free DNA was isolated from the post centrifugation supernatant obtained after cell block processing and combined with remaining material obtained after ThinPrep slide preparation. Molecular assays based on PCR product sizing, Sanger sequencing, and/or targeted-exome hybrid-capture NGS were concurrently performed and compared with matched tissue specimens.

Results: Total DNA recoveries, measured by absorbance, from the 48 cases ranged from 550 ng to 33.9 ug (mean = 5.1 ug, median = 2.9 ug) with 1 technical failure (Fig. 1). Twelve paired cases tested by size comparison of PCR products in EGFR

and ERBB2 yielded identical results. Three paired cases tested by Sanger sequencing for EGFR T790M yielded identical results. Ten paired cases tested by targeted-exome hybrid-capture NGS resulted with identical small insertion-deletion mutations at similar variant frequencies (+/- 2%). In addition, the conversion rate per unit input DNA to sequenceable adaptor-ligated library was 12.5 fold for cytology materials while 7.7 fold for FFPE specimens (p-value = 0.014).

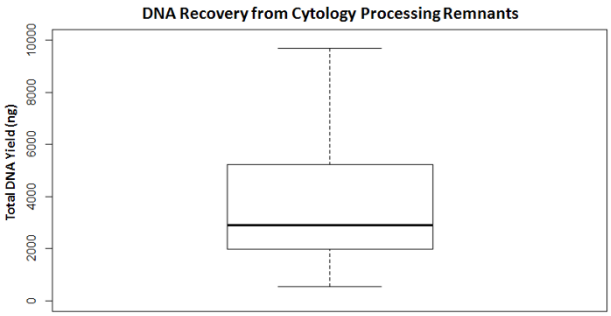

Conclusions: Residual cytology material can be used for molecular studies, without compromising diagnostic material availability. The higher conversion rate of cytology sourced DNA for NGS libraries suggests superior DNA quality compared to FFPE tissue. This can translate to lower DNA input cutoffs and the potential to accommodate patients with limited biopsy materials.

2076 Combined Molecular Testing (Mutational Analysis and MicroRNA Panel) of Thyroid Nodules Can Be Accomplished on Fine Needle Aspirate Slides

Maria L Torres, Angela M Sanguino Ramirez, Sydney D Finkelstein, Jan Silverman. Allegheny Health Network, Pittsburgh, PA; Redpath / Interpace Diagnostics, Pittsburgh, PA.

Background: Molecular analysis of indeterminate thyroid nodule specimens has been shown effective as an adjunct test. Two separate approaches are available: 1) mutation detection with high positive predictive value (PPV) and 2) a panel of microRNA (miRNA) that distinguished benign versus malignant disease with high negative predictive value (NPV). Molecular analysis has traditionally been carried out on fresh needle aspirated samples, requiring the collection of a separate specimen for this test. Our study shows that both approaches can be performed in microdissected stained fine needle aspirate (FNA) slides.

Design: Stained FNA slides and corresponding formalin fixed paraffin embedded (FFPE) tissue sections were collected on 15 patients with indeterminate thyroid nodule cytology. Microdissection of two separate sites was done under stereoscopic observation. Total nucleic acids were extracted and evaluated by next generation sequencing (NGS) for point mutations in BRAF, HRAS, KRAS, NRAS, PIK3CA genes and translocations of PAX8/PPAR and RET/PTC genes. In parallel, 10 marker microRNA profiling, designed to classify benign vs. malignant disease, used miR-29b-1-5p, miR-31-5p, miR-138-1-3p, miR-139-5p, miR-146b-5p, miR-155, miR-204-5p, miR-222-3p, miR-375, and miR-551b-3p. Statistical analysis compared performance as determined by surgical pathology outcome.

Results: All 15 cases yielded adequate levels of good quality DNA for duplicate NGS and miRNA analyses. BRAF mutation was detected in five patients with papillary thyroid cancer (PTC). One PTC was mutation negative, however, miRNA was positive. Duplicate testing showed significant variation in mutation clonality with close values for miRNA classifier. Of note, mutational clonality was consistently higher in the microdissected FFPE samples compared to microdissected cytology, however, miRNA classifier was equivalent in all microdissection targets.

Conclusions: Microdissection-based molecular analysis is demonstrated to be effective using residual cytology and FFPE slides. Sufficient levels of microRNA are available for detailed classifier determination. By combining both approaches, high PPV and NPV can be achieved while at the same time enabling close correlation between microscopic and molecular findings.

2077 Calretinin-Positive Lung Adenocarcinoma: An Ultrastructural Study

Ivonne Vazquez, Raquel Albero, Lorena Diaz, Nuria Juanpere, Lara Pijuan, Teresa Baro, Sergio Serrano, Josep Lloreta. Consorci Sanitari Parc de Salut Mar, Hospital del Mar, Barcelona, Spain; University Pompeu-Fabra, Barcelona, Spain; Autonomous University of Barcelona, Barcelona, Spain.

Background: Calretinin is a calcium transporting protein characteristic of mesothelial cells as well as of steroid secreting cells of the adrenal gland, ovary and testes. It has been reported to be positive in up to 23% of lung adenocarcinomas. This is the first ultrastructural report of calretinin-positive adenocarcinoma.

Design: The index case was a left lung tumor from a 79 year-old patient with a history of papillary carcinoma of the thyroid. The tumor was worked up at the referring hospital and was sent for ultrastructural examination because of paradoxical immunohistochemistry (IHC) and histopathology findings. Subsequently calretinin antibody (SP65, Ventana, Roche®) was tested in a TMA containing 130 lung adenocarcinoma samples. The index case and the three positive cases detected in the TMA were processed for electron microscopy (EM).

Results: The index case had a light microscopic appearance suggestive of adenocarcinoma (ADC) but with IHC strong calretinin positivity was detected in the nucleus and the cytoplasm of many tumor cells. In addition tumor cells expressed HBME-1 (pericellular pattern), cytokeratin 7 and were negative for TTF1, napsin and thyroglobulin. By EM, tumor cells showed abundant, short microvilli with pericellular distribution as well as junctional complexes, typical of ADC. Three of 130 ADC in the TMA (2.3%) were positive for calretinin, although in a smaller number of cells than the index case. By EM, one of these cases showed classical features of glandular differentiation without pericellular microvilli. The remaining two cases were solid ADC in which EM showed only very focal and poorly preserved glandular differentiation. All the cases had in common the presence of complex invaginations of the nuclear membrane, often associated to one or several large nucleoli.

Conclusions: Calretinin positivity is very unusual in lung ADC but can result in diagnostic problems. It is advisable to use EM as the complementary technique in any lung tumor with paradoxical IHC results. We have not found common features in our cases that can be associated to "aberrant" calretinin positivity but all of them had similar nuclear and nucleolar features indicative of high nuclear pleomorphism and nucleolar hyperactivity.

2078 Pathological Staging of Fibrosis by High-Resolution Magnetic Resonance Imaging of Liver Microarchitecture

Mark Valasek, Vera Vavinskaya, Mojgan Hosseini, Claude Sirlin, Graeme Bydder, Nicklaus Szeverenyi. University of California San Diego, San Diego, CA.

Background: Magnetic Resonance microscopy (MRM) of tissues provides enhanced spatial resolution over clinical MRI (100-10,000 times) - similar to low-power light microscopy - allowing for detailed correlation of histology with MR properties. Here, we utilize an MRM method to stage liver fibrosis.

Design: Nine formalin-fixed human hepatic specimens were examined with an 11.7T small bore MR system (Buker BioSpin Billerica MA) using solenoid coils of 6-11mm diameter. Spin echo (SE), Gradient echo (GE), Diffusion weighted (DW), Ultrashort TE (UTE), and ZeroTE (ZTE) sequences were performed at high spatial resolution (voxel size 15µm). 2-dimensional gray-scale and pseudo-color images of each sample were generated prior to routine histological processing and staining. The MR images were independently evaluated for fibrosis stage by 3 hepatopathologists untrained on MR and blinded to the histologic fibrosis stage.

Results: The human hepatic lobule was easily identifiable by MRM. Fibrosis produced a shortening of T_1 and an increase in T_2 and T_2* with signal concentrated around the portal tracts. In cirrhosis, there were variably sized nodules with surrounding thickened septa showing highly anisotropic diffusion restricted perpendicular to the plane. After scanning, standard histologic staging revealed livers with the following: 4 with no fibrosis, 1 with stage 2 fibrosis (Batts and Ludwig), 1 with stage 3 fibrosis, and 3 with cirrhosis. On inaugural evaluation of MR imaging, all three pathologists accurately agreed on 2 of the 9 samples, both of which were examples of cirrhosis. 5 of 9 samples had two pathologists in agreement, and 2 of 9 samples had no agreement. Despite incomplete agreement, lower histologic fibrosis stages generally had lower MR imaging fibrosis stages for each of the pathologists.

Conclusions: MR microscopy is capable of visualizing hepatic microarchitecture in both normal and fibrotic livers. The lobular microarchitecture and the highly anisotropic nature of fibrosis have not previously been visualized with MRI. In addition, fibrosis and cirrhosis can be recognized on MR imaging by pathologists, even without prior training on MR. Improvements in MR sequences, higher resolution, and greater experience in evaluating such images are likely to improve agreement. Overall, the correlation of MR microscopy and histology utilizes both pathological and radiological expertise and will provide an opportunity to enhance translation of new tissue visualization techniques into the clinical domain.

2079 Whole-Exome Sequencing Identifies a Homozygous POLG2 Missense Variant in an Infant with Fulminant Hepatic Failure and Mitochondrial DNA Depletion

Hemant Varma, Phyllis L Faust, Peter L Nagy, Alejandro D Iglesias, Stephen M Lagana, Karen Wou, Michio Hirano, Mahesh Mansukhani, Kirsten E Hoff, William C Copeland, Ali B Naini. Columbia University Medical Center and New York Presbyterian Hospital, New York, NY; National Institute of Environmental Health Sciences, NIH, Research Triangle Park, NC.

Background: Mitochondrial DNA depletion syndrome lead to diverse early-onset diseases that affect skeletal muscle, brain and liver function. Mutations in several nuclear DNA-encoded genes can lead to mitochondrial DNA depletion. We report a case of a 3-month-old boy who presented with hepatic failure, and was found to have severe mtDNA depletion in the liver and muscle.

Design: Whole-exome sequencing was performed on DNA derived from the patient's peripheral blood using Illumina Next-Generation sequencing and our in-house analysis pipeline.

Results: We identified a homozygous missense variant (c.544C>T, p.R182W) in the accessory subunit of mitochondrial DNA polymerase gamma (*POLG2*), which is required for mitochondrial DNA replication. This variant is predicted to disrupt a critical region required for homodimerization of the POLG2 protein, and cause a loss of processive DNA synthesis. Both parents were phenotypically normal and were heterozygous for this variant.

Conclusions: This case is the first report of a homozygous mutation in *POLG2*, and adds POLG2 to genes causing mitochondrial DNA depletion syndrome presenting with hepatic insufficiency. This also demonstrates the clinical utility of whole-exome sequencing in disease gene discovery.

2080 Digital Image Analysis Requires the Supervision by the Pathologist: A Study on Immunohistochemical Scoring

Pamela Villalobos, Edwin Parra, Barbara Mino, Kathryn O'Donnell, Jaime Rodriguez-Canales. MD Anderson Cancer Center, Houston, TX; UT Southwestern Medical Center, Dallas, TX.

Background: Digital image analysis (DIA) is an increasingly important tool for research and diagnostic pathology, specially on the analysis of immunohistochemical (IHC) expression, with the advantages of saving time to the pathologist and improving the reproducibility by decreasing inter-observer variation. The current advances in DIA technologies suggest that IHC scoring could be an automated process. The aims of this study are to compare the scoring reproducibility of IHC expression evaluated by optical microscopy by a pathologist (OM), by an digital image analysis system including a pattern recognition software (DIA), and by digital image analysis supervised by pathologists (SDIA), and to identify potential pitfalls in the different methods.

Design: A tissue microarray set of 218 patients (3 cores of 1 millimeter diameter per patient) with Non-Small Cell Lung Carcinoma was selected from the archives of the Department of Pathology at MD Anderson Cancer Center. IHC membrane expression of Protocadherin-7 (PCDH7) on the cancer cells was evaluated by 3 methods using H-score system: 1) light microscope (OM) by 2 pathologists; 2) DIA with Aperio Image Toolbox™ using a membrane-specific algorithm on tumor cells selected by a pattern recognition software (GENIE™, Aperio); and 3) SDIA, using the same DIA method but supervised by 2 pathologists reviewing and correcting the computer during and after after image analysis.

Results: The correlation between the IHC score by DIA compared with the pathologist (OM) was r= 0.401 (P <0.001). SDIA showed a better correlation with pathologist scoring (r= 0.882, P < 0.001). SDIA showed also better sensitibity and specificity than DIA (100% and 21%, versus 83% and 10%, respectively). Overall DIA showed higher IHC scores (p=0.0001), due to misinterpretation of false staining and cell type by the image pattern recognition software employed.

Conclusions: Digital image analysis is important tool for the pathologist in both, research and clinical settings. However, our findigns confirm that the digital image analysis needs the supervision by the pathologist during the process to assure the quality control of the IHC interpretation, enhancing thus the specificity of the IHC data. Supervision by a pathologist may be of utmost importance for the application of image analysis tools in diagnostic pathology.

2081 Comparison of Three TTF-1 Antibody Clones on Non-Small Cell Lung Carcinomas with Correlation of IHC Expression, mRNA Levels and Patient Outcome

Pamela Villalobos, Carmen Behrens, Edwin Parra, Barbara Mino, Jaime Rodriguez-Canales. MD Anderson Cancer Center, Houston, TX.

Background: TTF-1 immunohistochemical (IHC) expression is a key diagnostic marker to differentiate lung adenocarcinoma (ADC) from squamous cell carcinoma (SCC). TTF1 antibodies have been reported to exhibit different specificity, with clone 8G7G3/1 showing better results. We investigated the TTF1 IHC expression in lung cancer comparing 3 clones and correlated IHC data with *NKX2.1* mRNA expression and patient outcome.

Design: A tissue microarray (TMA) containing samples from 163 patients (113 ADC & 50 SCC) was employed. TTF1 expression was evaluated by IHC with 3 monoclonal antibodies: 8G7G3/1, SPT24 and EPR5955. Nuclear TTF1 expression on tumor cells were scored by 2 pathologists using H-score. Expression of *NKX2.1* mRNA were obtained from microarray data (Gene Expression Omnibus repository) from frozen tumor tissue corresponding to the same tumors of the TMA. Patient's outcome data was retrieved from the clinical records.

Results: TTF1 IHC expression in all cases with clones SPT24 & EPR5955 were comparable with clone 8G7G3/1 (r=0.877 & r=0.899 respectively, P< 0.001). The 3 clones detected the same ADC positive cases (n=103) and negative cases (n=9). However, clones SPT24 & EPR5955 labeled a higher number of SCC than 8G7G3/1 (28%, 22% & 10% respectively, p<0.0001). In ADC cases, TTF1 IHC expression with clones 8G7G3/1, SPT24 & EPR5955 showed a correlation with *NKX2.1* mRNA (r= 0.563, r=0.457 & r=0.435 respectively, $P < 0.001$); however, there is poor correlation between the IHC & mRNA expression in the SCC group with all 3 antibodies (r= 0.275, r=0.248 & r=0.157 respectively, $P < 0.001$). Kaplan–Meier analysis showed that a positive TTF1 IHC expression in ADC cases using clones 8G7G3/1 & SPT24 correlated with better overall survival (OS, *P= 0.01965 and P= 0.05* respectively, univariate analysis). We did not find correlation between patient outcome and TTF1 IHC expression in the SCC group.

Conclusions: Our findings show that all 3 studied TTF1 antibodies were comparable for the detection of ADC cases. We confirmed previous findings that clone 8G7G3/1 is more specific for the diagnosis of ADC, as it detects less SCC positive cases, making this clone more useful for diagnostic purposes. Despite that we found poor correlation between TTF1 IHC expression and mRNA, we think that the detection of SCC positive cases still needs further investigation to clarify its biological meaning and the possible utility of clones SPT24 & EPR5955 for scientific purposes.

2082 Numbered Agar Bodies to Individualize Needle Biopsy Specimens - A Paradigm Shift in Specimen Identification

Ulrich Vogel. University Hospital of Tuebingen, Tuebingen, Baden-Wuerttemberg, Germany.

Background: Specimen mix-up in the histology laboratory is a fortunately rare, but potentially devastating source of medical error concerning biopsy specimens of different organs. The main reason why it is difficult to detect the accidental switching of tissue specimens is the fact that normally not the tissue itself but the sample container (e.g. transportation containers, embedding cassettes, slides) is marked. To achieve a real individualization of the specimens, I propose the use of numbered agar bodies with slots into which needle biopsy specimens can be inserted and secured with liquid agar.

Design: Standard steel embedding molds for pouring paraffin blocks were filled with liquid agar. Before solidification of the agar spacer bars and a random set of spacer figures (base area: 3 mm^2/figure) were put into the mold. After solidification of the agar the spacers were removed. The figure slots were filled with a mixture of liquid agar, dye of different colors and protein (e.g. fine minced meat). After solidification, the numbered agar bodies were stored in formalin 4% until the slots were filled with needle biopsy specimens.To firmly attach the specimens to the surrounding agar body liquid agar was poured onto the specimens. The agar block was routinely paraffinized, cut and stained.

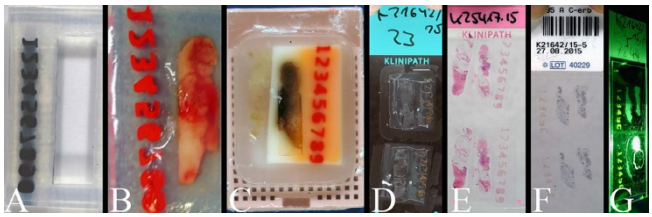

Results: Agar bodies could be successfully individualized by filling the figure slots with a colored agar-protein mixture. At all steps of processing, the number was clearly visible to the naked eye (Figure 1 A-G: Different specimens). This was especially true for the unstained and stained sections. The number remained on the slide even at immunohistochemistry and fluorescence in situ hybridization. The needle biopsy specimens could be securely fixed to the surrounding agar by using liquid agar. This liquid agar (55°C) did not harm the immunoreactivity of the unfixed tissue specimens.

Conclusions: By using numbered agar bodies with firmly attached needle biopsy specimens it is possible to individualize the specimens theirselves and not only the specimen containers. Therefore, the specimens can be clearly identified at all steps of processing and evaluation making specimen mix-ups extremely unlikely.

2083 Hepatitis C Virus Genotyping Using Next-Generation Sequencing—An Efficient and Cost-Effective Alternative to Sanger Sequencing in the Hospital Laboratory Setting

Cameron Wales, George Corpus, Dimitri Gonzalez, Chalom Sayada, Chung-Che Chang. UCF, Orlando, FL; ABL SA, Luxembourg, Luxembourg; Florida Hospital, Orlando, FL.

Background: Testing for Hepatitis C Virus (HCV) genotype is recommended to guide selection of the most appropriate antiviral regimen. In clinical laboratories this has traditionally been carried out using PCR and first generation (Sanger) sequencing based technologies. We evaluated the performance characteristics of Next Generation Sequencing (NGS) in regards to HCV genotyping in order to increase speed, reduce cost, and to generate more accurate co-infection profiles.

Design: RNA was extracted from plasma samples of individuals with HCV and subsequently amplified using primers targeting the NS5B gene. Following reverse transcription and Nextera library preparation, the libraries were loaded onto a primed MiSeq flow cell. Read quality control was ensured using tools provided within the Illumina platform. HCV genotyping was carried out using the following tools: PathGEN® PathSEQ® Virome, ABL SA - DeepChek®-HCV and FH-HCV-GT. Samples were simultaneously sent to a reference laboratory for Sanger sequencing. To measure our techniques ability to detect co-infection of different strains of HCV, samples of HCV type 1a and 3a were mixed to simulate 50%, 10% and 5% co-infection.

Results: Turnaround time is 24 to 48 hrs using our NGS technique as compared to 9-11 days using the reference laboratory. Cost per sample, including reagents and tech time, is $68 processing 30 samples at a time using our NGS technique, with the potential cost of $21 processing 96 samples at a time with further optimization, as compared to $300 per sample using the reference laboratory. In comparison, the reagent cost of Sanger sequencing is closer to $30 per sample but the throughput is only 16 samples per run. There was 100% concordance of genotypes with the Sanger method with 16,000 reads or greater using ABL SA - DeepChek®-HCV and FH-HCV-GT.

The preliminary results from the mixing study indicate the ability to detect 50% co-infection.

Conclusions: Our data indicates that HCV genotyping by NGS technology is as accurate as Sanger sequencing, the current gold standard. It indicates that it is more cost-effective and provides a shorter turnaround time. Additionally, the NGS technology was able to detect co-infection of different strains of HCV. There is tremendous potential for the application of NGS in the hospital laboratory setting for cost savings, efficiency, as well as for more accurate clinically relevant genotyping information.

2084 Direct IHC by Using PolyHRP Labeled Trastuzumab (Herceptin) - A Potential New Companion Diagnostic Test for Herceptin Treatment

Li Juan Wang, Yihong Wang, Song Q Zhao, Yonghua Zhang, Zhiqing Zhang. Brown University Alpert School of Medicine, Providence, RI; St Mary Hospital, Madison, WI; Novodiax, Hayward, CA.

Background: In this pilot study, we have compared the performance of Novodiax's PolyHRP-trastuzumab on archived FFPE breast cancer tissues with the results of Dako HercepTest (IHC) and HER2 FISH.

Design: Trastuzumab was labeled with Novodiax's PolyHRP by following a Direct IHC antibody labelling protocol (Patent pending). The incubation condition of the PolyHRP-trastuzumab on tissues was 30 min at room temperature.

Results: Novodiax's PolyHRP-trastuzumab was first titrated on multiple HercepTest 3+ and 0 tissues to obtain an optimal working concentration. We did not observe a broad range of staining intensity based on the tissue sample set we tested, therefore a simple positive or negative scoring system was used in this pilot study.

Dako HercepTest IHC (No Tissue)	Dako HER2 FISH (no Tissue)	Novodiax PolyHRP-trastuzumab (No Tissue)
3+ (8)	Not tested	+ (5)
		- (3)
2+ (12)	+ (1)	+ (1)
	- (11)	- (11)
1+ (11)	Not tested	- (11)
0 (2)	Not tested	- (2)

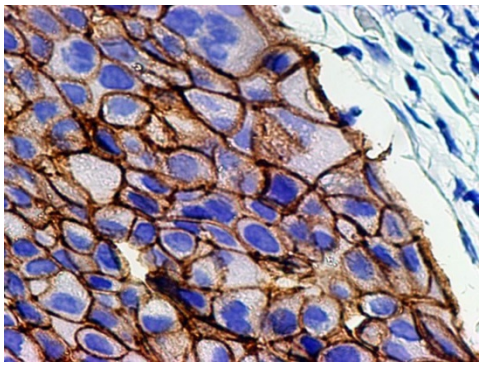

100% of cancer cells showed positive membrane staining by polyHRP-trastuzumab in this HercepTest 3+ tissue.

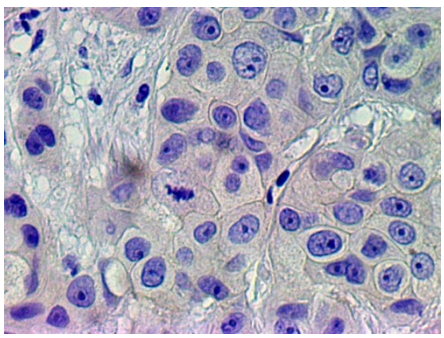

None of cancer cells showed positive membrane staining by polyHRP-trastuzumab in this HercepTest 3+ tissue.

Conclusions: PolyHRP-trastuzumab showed 100% concordance with FISH on the HercepTest 2+ tissues (See the Table) and therefore may be considered as a simpler, cost-effective and more reliable alternative for both IHC and FISH products in the current market in near future. Surprisingly, three of the eight (37.5%) HercepTest 3+ tissues were tested negative by PolyHRP-trastuzumab.

2085 RNAscope® 2.5 Duplex - A Robust High Performance Chromogenic Duplex RNA In Situ Hybridization Technology

Li-chong Wang, Bingqing Zhang, Casey Kernag, Daniel Kim, Henry G Lamparski, Nan Su, Xiao-Jun Ma, Yuling Luo. ACD, Inc, Hayward, CA.

Background: RNAscope® (Advanced Cell Diagnostics, Inc) is an RNA in situ hybridization (ISH) technology with a unique signal amplification and background suppression strategy. It is capable of detecting single RNA molecules in the native context of tissue and cellular structure in a variety of sample types, including formalin fixed paraffin embedded (FFPE) tissues. The ability to detect two RNA species simultaneously in a chromogenic assay is highly desirable in a variety of biomarker research and diagnostic applications. Here we report a highly sensitive and robust chromogenic duplex assay, RNAscope 2.5 duplex.

Design: The RNAscope 2.5 duplex assay was based on an improved RNAscope core technology which features a novel target retrieval method, an improved signal amplification structure, and more robust reagent formulation. It utilizes a sequential signal amplification strategy to achieve high sensitivity and signal-to-noise ratio in both detection channels with well preserved tissue morphology. Furthermore, we have applied the same duplex technology as a fully automated assay on the Leica Bisoystems' BOND Rx system. To evaluate the detection robustness of the RNAscope 2.5 duplex assay, we tested several clinically relevant biomarker combinations in various human FFPE sample types, including breast, cervix, larynx, lung, lymph node, skin, and stomach.

Results: With the RNAscope 2.5 duplex assay, the two detection channels (red and black for the manual assay, and red and dark brown for the Leica Biosystems' BOND Rx) generate distinct color precipitates on the blue hematoxylin counter stain background, which allows easy recognition of signals from two different biomarkers in the context of tissue morphology. Distinct and specific signal was observed for each of the markers only in the expected cell types, demonstrating high specificity of the RNAscope® probes. In contrast, staining with a negative control probe yielded essentially no background signal in all the human tissues tested, showing a high signal-to-noise ratio. Importantly, there was no loss in signal from either detection channels in the duplex format compared to the standard single channel assays.

Conclusions: The RNAscope® 2.5 duplex assay allows robust simultaneous detection of two RNA biomarkers in morphological context. The fully automated assay is an ideal high-throughput tool for studying expression and spatial relationships of various biomarkers in various sample types.

2086 Novel 3-D Exploration and Analysis Tool for Surgical Pathology Specimens

Seth Winfree, Tarek El-Achkar, Kenneth Dunn, Carrie L Phillips. Indiana University, Indianapolis, IN.

Background: Analysis of surgical pathology specimens is primarily based on two-dimensional (2-D) histological sections of thinly-sliced tissue. As such, histopathological interpretation of three-dimensional (3-D) structures may be inherently influenced by 2-D sampling bias. Pathologists frequently rely on tedious manual counting to quantify infiltrating cells or qualify heterogeneous cell types in multiple 2-D microscopy fields. This laborious and subjective process is time consuming and may not be reproducible. Furthermore, manual sectioning of tissue with a microtome knife destroys neighboring tissue architecture. We sought to develop a reliable, objective and automated system to overcome these limitations.

Design: We developed and employed in situ, 3-D tissue cytometry (TC) to explore and analyze different cell types in thick biological tissues. Tissue was labeled with fluorescent antibodies and markers, from which optical Z-stacks of 2-D images were digitally collected by confocal fluorescent microscopy. We created custom analysis and processing plugin tools on the NIH ImageJ platform that allowed us to recognize, segment and select specific cells and groups of cells based on nuclear and cytoplasmic segmentation in 3-D.

Results: Using rodent and human kidney specimens, we used TC to provide quantitative spatial and structural information. We resolved different cell populations based on cell surface markers. In a mouse model of macrophage depletion, TC reproduces flow cytometry data. TC was also used in an "exploration mode" that allowed for discovery of innovative metrics not obvious by conventional 2-D methods. For example, we used TC to uncover a novel population of renal epithelial cells expressing dendritic cell marker CD11c.

Conclusions: 3-D TC is a precise and accurate tool that could be readily adapted to the field of anatomic pathology, thus enabling the accurate, efficient and standardized analysis of complex tissue characteristics. The rendering of an accurate and reproducible diagnosis has an overall benefit of improving patient safety.

2087 Mass Spectrometry of Formalin-Fixed Paraffin-Embedded Tissue: Proteome, Phosphoproteome and Histone Post-Translational Modifications

John Wojcik, Simone Sidoli, Benjamin A Garcia, Kumarasen Cooper. Hospital of the University of Pennsylvania, Philadelphia, PA; University of Pennsylvania, Philadelphia, PA.

Background: A major obstacle to the proteomic analysis of human diseases is the availability of well-characterized fresh tissue. Formalin-fixed, paraffin-embedded (FFPE) tissues in pathology archives are a potential alternative. FFPE tissue however, has not been widely used for such studies due to difficulties with protein isolation. We present a protocol that allows for mass spectrometry based protein analysis of FFPE tissue with a comparable sensitivity to fresh tissue analysis. Moreover, our protocol is suitable for phosphoproteome and histone post-translational modification (PTM) characterization.

Design: Fresh tissue was collected from autopsy liver specimens and snap frozen in liquid nitrogen or fixed according to standard histopathology protocols. Fresh tissue was lysed and homogenized; FFPE tissue was subjected to deparaffinization, antigen retrieval, lysis and homogenization under varying conditions (20 total samples). Proteome, phosphoproteome (enriched using TiO_2) and histone specimens were analyzed using nano-liquid chromatography and tandem mass spectrometry. Peptides were identified and label-free quantified using MaxQuant. Histone PTMs were identified and quantified by peak integration using lab-developed software. Fresh and FFPE results were compared using Pearson's correlation coefficient and statistical assessment of bias in identified peptides was based hypergeometric distribution of gene ontology annotations (DAVID and GOrilla software tools).

Results: Across twenty samples and conditions, we identified and quantified 2526 proteins and 2432 phosphopeptides. The best-performing protein extraction protocol for FFPE and fresh liver specimens yielded peptide identifications from 2067 and 2106 proteins, respectively. Comparison of gene ontology annotations revealed no biases between proteins or phosphopeptides identified in FFPE versus fresh tissues. The number of proteins and phosphopeptides 'missed' in FFPE compared to fresh tissue was low and included only low abundance signals, suggesting that the differences were stochastic. Quantification of histone PTMs from FFPE and fresh tissue were in excellent agreement (R=0.88), indicating that our protocol is applicable to both proteomics and epigenomics studies

Conclusions: We optimized a mass spectrometry based protocol which allows the analysis of the cellular proteome, phosphoproteome and histone PTMs in fresh and FFPE tissues in a comparable manner.

2088 Drug Induced Phospholipidosis in Kidney: Ultrastructural Features

Guanjun Xia, Sirma Koutzaki, Shahad Abdulameer, Shraddha Patel, Suganthi Soundararajan. Drexel University College of Medicine, Philadelphia, PA.

Background: Drug induced phospholipidosis (DIPL) is considered to be an acquired lysosomal storage disorder due to an adaptive response to cationic amphiphilic drugs (CADs) and toxic effects of gentamycin. DIPL is characterized by excessive accumulation of phospholipids in different organs mimicking the myelin figures (myelinoid bodies). In the kidney, Fabry disease, metabolic diseases and DIPL are known to cause myelin figures. Among the over 50 marketed CADs, only a few have relevance in the kidney. Thus, renal DIPL is rare and could lead to diagnostic difficulty, particularly due to the lack of specific staining on light microscopy. Renal DIPL identified by electron microscopy (EM) is the diagnostic hallmark.

Design: In our EM pathology database (2008-2015), three native kidney biopsies with DIPL were identified. There were 3 adults (1 male: 2 females) with an age range from 54 to 74 years. The histological sections, toluidine blue stained thick sections and electron micrographs were reviewed.

Results: Ultrastructural studies showed characteristic cytosolic inclusions consisting of myelin- like lamellated structures resembling zebra bodies or lamellar bodies in the expanded podocyte cytoplasm and Bowman's space in all three patients.

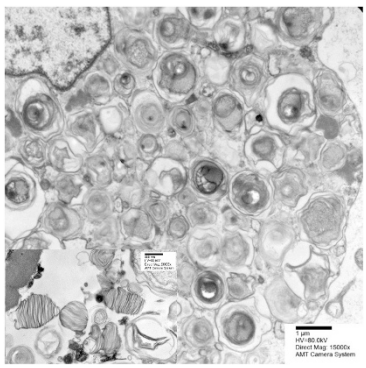

Lamellated structures were present in the tubular epithelium in one patient. Hypersensitivity-type tubulo-interstitial nephritis was present in two patients. Other significant coexisting pathologic diagnoses include recent diagnosis of SLE, membranoproliferative glomerulonephritis with C3 deposits, hypertensive and diabetic nephropathy. Multiple drug intake history was present in all patients, cocaine abuse in two of them and azithromycin in one patient; cocaine and azithromycin are CADs. No evidence of clinical Fabry disease, previous metabolic inclusion diseases or chloroquine intake was identified.

Conclusions: Ultrastructural discovery alone of DIPL has been approved to be the essential criteria in diagnosing this rare disease. In the kidney, diagnostic myelin figures are located within the lysosomes of the podocytes and the tubular epithelium. Pathologists should be aware of these inclusions, caused by pharmacological/recreational agents, in the absence of clinical Fabry disease.

2089 Locking Tissue Orientation from Grossing through Microtomy Using Orientation Gels

Douglas T Yamanishi, Lydia E Figueroa, Cliff Hom, Carlos Sanchez, Luis Chavez, Julie A Galindo, Erico von Bueren. Sakura Finetek USA, Inc., Torrance, CA.

Background: Pathologists, Pathologist Assistants and Histologists are challenged with orienting and locking small tissue specimens like biopsies or core punches in cassettes at grossing and embedding. If not oriented correctly, the tissue sections may not be adequate for the Pathologist to diagnose and require time consuming re-work. Sakura developed the Tissue-Tek® Paraform® Orientation Gels for locking location and orientation of specimens at the time of grossing thus eliminating the need to orient the processed specimens downstream during manual or fully automated embedding. The grossed biopsies and small specimens such as shaves, arteries or nerves are placed into the easy-to-use, precast gels in the desired orientation, then the cassette lid is closed locking the orientation. Finally the oriented cassette is processed and embedded without further manipulation. The matrix of the Orientation Gels is dyed to maximize contrast with the specimens and to increase specimen throughput in grossing.

Design: A study was performed to confirm that the Orientation Gels lock the location and orientation of specimens from grossing to microtomy. Specimens were either small or core needle biopsies. The specimens were processed and embedded. The specimen blocks were sectioned, stained (Hematoxylin and Eosin, IHC and ISH) and coverslipped. The location and orientation of all biopsies and small specimens in the Orientations Gels was documented from grossing through staining by photographs taken at the end of each processing step and by calculation of the newly developed Specimen Immobility Score.

Results: Orientation Gels used in combination with the Paraform Biopsy Cassettes lock the location and the orientation of specimens keeping them in one plane, preventing specimen migration (movement) or loss and re-embedding.

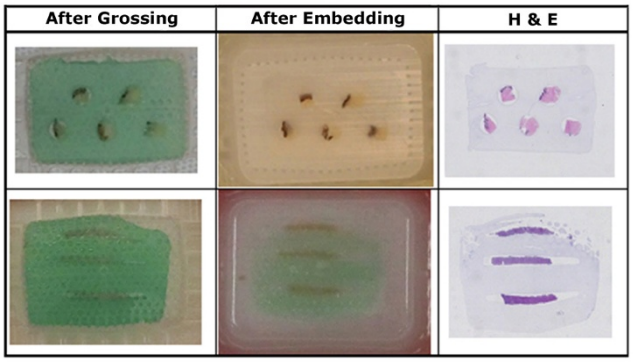

Conclusions: This study shows the utility of Orientation Gels to lock specimen location and orientation from grossing through microtomy. They enable flexible and customizable tissue orientation and accommodates multiple tissue types (e.g. core biopsies, punch biopsies, shaves, arteries, nerves). Orientation Gels represent a new valuable tool for Pathologists and Pathology Assistants to standardize the pre-analytical process, prevent loss of specimens and avoid re-embedding.

2090 High Efficiency Prostate Biopsy Evaluation after Training Using Full-Field Optical Coherence Tomography

Chongqing Yang, Eugenie Dalimier, Anil Parwani, Riccardo Riccio, Nicolas Barry Delongchamps, Arnaud Duc. LLTech SAS, Paris, France; Ohio State University, Columbus, OH; Hôpîtal Cochin, Paris Descartes University, Paris, France; Beijing Hospital of Health Ministry, Beijing, China.

Background: The diagnosis of prostate cancer involves multiple randomized biopsies, leading to over-diagnosis and over-treatment, as well as unnecessary non-informative samples. Full-field optical coherence tomography (FFOCT) is a new optical imaging technique that offers high-resolution (1µm in all 3 directions) in-depth images of gross tissue, approaching traditional histological sections. It can allow in-situ, quick analysis of cores just after biopsy, in particular when MRI-targeted. Recent studies have emphasized the essential learning process for clinicians to fully apprehend this novel imaging modality. This study aimed to define standard reading criteria for the benign/malignant classification on FFOCT images of prostate biopsies, and test the reading criteria amongst doctors.

Design: A set 25 images of prostate biopsies, in comparison with corresponding histological slides, was used to construct an atlas with emphasized specific benign and malignant structures. A set of reading criteria was defined. After training on the atlas, pathologists and urologists were asked to blindly analyze another set of 113 FFOCT biopsy images, notify the presence/lack of malignant structures and state on the malignancy of the biopsy.

Results: In the blinded study, pathologists and urologists obtained very high accuracy scores, above 90%, when compared to the histological diagnosis of the biopsies.

Conclusions: FFOCT is as a fast and non-destructive imaging technique that provides a quick assessment of the tissue morphology and appears as a potential complementary tool for prostate cancer screening. After training, clinicians can be very efficient in reading the images to qualify the biopsies. The technique could be used on-site during the biopsy procedure to validate the cores, for more efficient prostate biopsies.

2091 Immunohistochemical Double and Triple Stain Strategies with CD8, CD103, PD-1, FOXP3 and CK8/18 in Colon Adenocarcinoma

Wei Yuan, Jillian Tyrrell, David Tacha. Biocare Medical, Concord, CA.

Background: Tumor-associated immune suppression can lead to defective T-cell mediated antitumor immunity. CD8+ T-cells play a critical role in host defense against cancers; however, the presence of antigen-specific CD8+ T-cells does not always imply that cancers are efficiently eliminated or indicate a good prognosis. Other biomarkers that identify tumor infiltrating lymphocytes (TILS) include CD103, PD-1 and FOXP3, all of which play important roles in T-cell activation, T-cell regulatory and programmed cell death checkpoints. Existing methods for detection, such as flow cytometry, can deliver either phenotypic information on homogenous samples, or give immunohistochemical information on a single biomarker. However, it would be advantageous to simultaneously visualize the distribution of multiple biomarkers in TILs and discriminate stromal tissue versus solid tumor. Therefore, the development of double or triple stains may be a good strategy to improve interpretation of co-expression patterns of multiple targets.

Design: Cases of formalin-fixed paraffin embedded colon adenocarcinoma were randomly selected and processed for immunohistochemistry. Both mouse and rabbit monoclonal antibodies to CD8, FOXP3, PD-1 and CK8/18 were evaluated in a side by side comparison. Antibodies were optimally tittered for single, double and triple stains. CK8/18 was used as a staining mask to differentiate tumor cells from stromal tissues. TILs expressing CD8, FOXP3, and/or PD-1 were stained with brown, blue, red or yellow chromogens.

Results: Double and triple stains with a CK8/18 staining mask coupled with CD8, CD103, FOXP3 and PD-1 antibodies were successfully established. All single stains versus double and triple stains gave equivalent results. Mouse monoclonal versus rabbit monoclonal antibodies showed comparable staining results. TILs in stroma tissue versus those in tumors cells were easily distinguished with the CK8/18 staining

mask. Co-expression of CD8 + CD103, and CD8 + PD-1 was easily visualized with two-color staining. Ratios of CD8+ TILs and FOXP3+ TILs were also easily accessed from a single tissue section.
Conclusions: The evaluation of TILS in colon adenocarcinoma is enhanced with double and triple stains. The CK8/18 staining mask helps to separate stromal tissues from tumor epithelial cells. Thus, this technique may help facilitate acquisition of important prognostic information and help support new strategies in target therapeutic treatment.

2092 Validation of Placental Preservation for Pathologic Examination Using the TissueSAFE Formalin-Free Vacuum-Sealing System

Richard J Zarbo, Michelle Felicella, Arthur R Gaba. Henry Ford Hospital, Detroit, MI.
Background: Placentas are the unloved specimens of Labor and Delivery (L&D) and Pathology. Most are normal and not seen in Pathology but require safe systems for storage and disposal. Placentas that require pathologic evaluation present numerous challenges of non-standardized ex vivo time, tissue preservation conditions, timed exposure to formalin-fixation, consumption of high volumes of formalin for proper fixation and expensive disposal of the specimen and associated bucket of bloody formalin as hazardous waste. To address these issues, we have validated a vacuum-sealed, formalin-free tissue handling system designed to originate from L&D with intent to control placenta preservation and transport to Pathology for histologic examination.
Design: 8 placentas were transported fresh from L&D to Henry Ford Hospital Pathology. Each was dissected according to protocol with 3 standard sections for immediate formalin fixation. Placentas were then sealed under low vacuum with the TissueSAFE system (Milestone Medical, Kalamazoo, MI) and retrieved for dissection and formalin fixation after storage in vacuum-sealed bags at 4 degrees for 24 hours (8 cases), 48 hours (4 cases) and 72 hours (4 cases). H&E stained slides were independently assessed by 2 placental pathologists using a 3 part scheme of 1) Adequate, 2) Less than optimal, or 3) Inadequate for histologic evaluation. This study was IRB-exempt.
Results: All 102 H&E slides were assessed adequate for histologic evaluation. No degradation of histologic detail was noted between fresh, formalin fixed to delayed fixation after 72 hours of vacuum-sealed cold storage.
Conclusions: This histologic validation of vacuum-sealed human placentas allows consideration of differently designed processes for tissue handling by caregivers and pathologists. Potential advantages are controlled preanalytic placenta preservation up to 3 days at refrigerator temperature. Controlled fixation of fresh sections from each preserved placenta markedly reduces the amount of formalin (approximately 1 gallon/placenta) ordinarily used to fix the entire placenta before gross examination. Reduction of formalin at the front-end process of initial fixation translates to reduced back-end disposal of formalin as expensive hazardous waste. Both reductions translate to financial savings to the healthcare system. In L&D practices, this may eliminate formalin from the unit. Additionally, most placentas require disposal and vacuum-sealing of individual specimens provides for a safe isolation and disposal avoiding a fetid waste receptacle in L&D.

2093 Optimization of Tissue Section Thickness for Evaluation of Mitotic Figures in Whole Slide Imaging (WSI)

Shabnam Zarei, Xuemei Wu, Sarah M Jenkins, William Flotte, Taofic Mounajjed, Thomas Flotte. Mayo Clinic, Rochester, MN; Brown University, Providence, RI.
Background: Digital pathology has been used in different settings of clinical care as well as pathology education and it continues to be an evolving field in pathology practice. There are many factors influencing the quality of digital images including the quality of tissue processing, tissue staining, tissue thickness
and the setting of the slide scanner. There is minimal data available on optimizing the quality of tissue sections used for whole slide scanning. Mitotic
figures are important in the evaluation of many specimens. This study assesses the effect of tissue thickness on the quality of the images of mitotic figures of proliferative endometrial tissue.
Design: Four cases of Formalin-Fixed Paraffin Embedded benign endometrial biopsy were cut at 2, 3, 4, 5, 6, 7 and 8 micron thickness and were
stained with routine H&E staining. Photomicrographs were taken with a conventional microscope with attached camera and an Aperio whole slide scanner from 3 different areas from each slide. The same area was pictured with both conventional and WSI methods. A total of 148 images, either paired by the same mitotic figures captured by different methods (conventional vs. WSI) or by different tissue thicknesses captured by the same method, were randomly arranged using random.org. Ten pathologists assessed the paired images for diagnostic quality of the mitotic figures and the degree of confidence of their choice scored from 1-5 (1: the least and 5: the most confident).
Results: The analysis of the data showed that the optimum tissue thickness for WSI is 4 microns. There were no differences in preferences for conventional or WSI images for thicknesses ranging from 2 to 6 microns but there was a preference for conventional images at 7 and 8 microns.
Conclusions: The 4-micron tissue section had the best diagnostic quality for detection of mitotic figures when using WSI images. The degree of confidence of our subjects didn't show any significant differences when choosing WSI over conventional method images at 2 to 6 microns. However, as the tissue sections get thicker, there are advantages to conventional microscopy due to the ability to focus on the most diagnostic plane. This study emphasizes that pre-analytic factors such as tissue thickness are important in the clinical implementation of digital pathology.